Check for updates

A Newly Identified Virus in the Family *Potyviridae* Encodes Two Leader Cysteine Proteases in Tandem That Evolved Contrasting RNA Silencing Suppression Functions

Li Qin,[a] Wentao Shen,[b] Zhongfa Tang,[a] Weiyao Hu,[a] Lingna Shangguan,[a] Yaodi Wang,[a] Decai Tuo,[b] Zengping Li,[a] Weiguo Miao,[a] Adrián A. Valli,[c] Aiming Wang,[d] Hongguang Cui[a]

[a]Key Laboratory of Green Prevention and Control of Tropical Plant Diseases and Pests, Ministry of Education and College of Plant Protection, Hainan University, Haikou, Hainan, China

[b]Institute of Tropical Bioscience and Biotechnology, Chinese Academy of Tropical Agricultural Sciences, Haikou, Hainan, China

[c]Centro Nacional de Biotecnología (CNB-CSIC), Madrid, Spain

[d]London Research and Development Centre, Agriculture and Agri-Food Canada, London, Ontario, Canada

Li Qin, Wentao Shen, and Zhongfa Tang contributed equally to this work. Author order was determined by ascending chronological order based on the time in which these authors started with the project.

ABSTRACT *Potyviridae* is the largest family of plant-infecting RNA viruses and includes many agriculturally and economically important viral pathogens. The viruses in the family, known as potyvirids, possess single-stranded, positive-sense RNA genomes with polyprotein processing as a gene expression strategy. The N-terminal regions of potyvirid polyproteins vary greatly in sequence. Previously, we identified a novel virus species within the family, *Areca palm necrotic spindle-spot virus* (ANSSV), which was predicted to encode two cysteine proteases, HCPro1 and HCPro2, in tandem at the N-terminal region. Here, we present evidence showing self-cleavage activity of these two proteins and define their *cis*-cleavage sites. We demonstrate that HCPro2 is a viral suppressor of RNA silencing (VSR), and both the variable N-terminal and conserved C-terminal (protease domain) moieties have antisilencing activity. Intriguingly, the N-terminal region of HCPro1 also has RNA silencing suppression activity, which is, however, suppressed by its C-terminal protease domain, leading to the functional divergence of HCPro1 and HCPro2 in RNA silencing suppression. Moreover, the deletion of HCPro1 or HCPro2 in a newly created infectious clone abolishes viral infection, and the deletion mutants cannot be rescued by addition of corresponding counterparts of a potyvirus. Altogether, these data suggest that the two closely related leader proteases of ANSSV have evolved differential and essential functions to concertedly maintain viral viability.

IMPORTANCE The *Potyviridae* represent the largest group of known plant RNA viruses and account for more than half of the viral crop damage worldwide. The leader proteases of viruses within the family vary greatly in size and arrangement and play key roles during the infection. Here, we experimentally demonstrate the presence of a distinct pattern of leader proteases, HCPro1 and HCPro2 in tandem, in a newly identified member within the family. Moreover, HCPro1 and HCPro2, which are closely related and typically characterized with a short size, have evolved contrasting RNA silencing suppression activity and seem to function in a coordinated manner to maintain viral infectivity. Altogether, the new knowledge fills a missing piece in the evolutionary relationship history of potyvirids and improves our understanding of the diversification of potyvirid genomes.

KEYWORDS HCPro, *Potyviridae*, potyvirus, cysteine protease, leader protease, RNA silencing suppression, viral viability

The *Potyviridae* family represents the largest group of plant-infecting RNA viruses and includes many agriculturally and economically important viral pathogens, such as potato virus Y, soybean mosaic virus, and plum pox virus (PPV) (1–4). A large majority of viruses in the family (here referred to as potyvirids) have one positive-sense single-stranded RNA genome (8.2 to 11.3 kb) and flexuous filamentous particles of 11 to 20 nm by 680 to 900 nm in size (2). Based on the genome composition and structure, sequence similarity, and transmission vector, potyvirids are currently sorted into the 10 following definitive genera: *Bevemovirus*, *Brambyvirus*, *Bymovirus*, *Ipomovirus*, *Macluravirus*, *Poacevirus*, *Potyvirus*, *Rymovirus*, *Tritimovirus*, and *Roymovirus* (2, 5). Exceptionally, bymoviruses have bipartite genomes (RNA1, 7.2 to 7.6 kb; RNA2, 2.2 to 3.6 kb) that are packaged into two modal particles of 250 to 300 nm and 500 to 600 nm in length (1, 2, 6). The genomes of all potyvirids, excluding bymoviruses, contain a single long open reading frame (ORF) and another relatively short ORF (PIPO) that results from RNA polymerase slippage in the P3-coding region (7–10). In particular, the same slippage event occurs in the P1-coding region of sweet potato-infecting potyviruses, given raise to an additional ORF (PISPO) (9, 11, 12). Upon translation, the resulting viral polyproteins are proteolytically processed by virus-encoded protease domains into 10 to 12 mature factors (5). Both the organization and sequence composition of potyvirid genomes from P3 to CP are relatively conserved (3, 5). However, the leader proteases encoded by the 5′-terminal regions vary greatly in number, arrangement, and sequence similarity (3, 5). Therefore, the polyprotein segment from P3 to CP is defined as the conserved central and carboxyl region, whereas the segment upstream of P3 is defined as the hypervariable N-terminal region (5).

The hypervariable N-terminal region contributes to the diversification of potyvirids (5). In fact, potyvirid genomes vary greatly in size, and this difference is mainly attributed to their hypervariable 5′-terminal regions (corresponding to the genomic RNA2 of bymoviruses) (5). This genomic region encodes one or two leader proteases arranged in a quite variable manner. Most potyvirids, including potyviruses, rymoviruses, brambyviruses, roymoviruses, tritimoviruses, poaceviruses, and a member of the *Ipomovirus* genus (sweet potato mild mottle virus [SPMMV]), share the same pattern of leader proteases, a chymotrypsin-like serine protease (P1) and a cysteine protease (HCPro) in tandem (1, 3, 5). However, P1 is missing and only HC-Pro is present in the N-terminal region of viruses from the *Macluravirus* and *Bevenevirus* genera, whereas HCPro is missing and either one or two P1s are present in ipomoviruses (except for SPMMV) (2, 3, 5). Remarkably, P1 and HCPro are the most divergent factors among all mature potyvirid proteins (3, 13–16). In the case of HCPro, for instance, its molecular mass ranges from ∼28 kDa in bymoviruses to ∼50 kDa in potyviruses and rymoviruses (5).

Besides the role as peptide cutters, proteases from plant viruses also function in different steps of the viral infection cycle (17–19). In recent years, several significant advances describing the biological roles of potyvirid leader proteases have been achieved. For instance, P1 can be sorted in two groups based on protein features and function: type A and type B (13), with those of the first group acting as important determinants in host adaption (5, 20–22). In turn, type B P1s (tested so far) display RNA silencing suppression activity (23–26). HCPro is a well-studied multifunctional protein that plays diverse roles during the viral infection cycle, including (i) plant-to-plant transmission, (ii) RNA silencing suppression, (iii) polyprotein maturation, and (iv) enhancement of viral particle yield (3, 27–32). Remarkably, whereas all these studies involved viruses from some, but not all, HCPro from different genera, the biological significance of HCPro from viruses in *Macluravirus*, *Brambyvirus*, and *Bymovirus* is largely unknown.

RNA silencing is a well-studied fundamental, evolutionarily conserved mechanism to regulate gene expression in eukaryotes and functions as a primary immune defense against viral infection in plants (33, 34). In turn, plant viruses have evolved to express viral suppressors of RNA silencing (VSRs) to counteract RNA silencing machinery (34). These VSRs vary highly in sequence, share no structural similarities, and interfere with specific steps of the RNA silencing pathway through a variety of mechanisms. Readers

are referred to several excellent reviews for more information (18, 34–36). HCPro from viruses in *Potyvirus* is a well-studied VSR protein. Most potyviral HCPro(s) suppress host RNA silencing via sequestrating 21- and 22-nucleotide (nt) small RNA of viral sequences (vsiRNA). Alternatively, others might perturb different steps of the RNA silencing pathway, such as inhibition of methylation of vsiRNA, interference with effector protein (AGO1), and disturbance of RDR6-mediated amplification of viral double-stranded RNA (3, 5). Nevertheless, RNA silencing suppression and its underlying mechanism of HCPro in other genera of the family have rarely been reported.

Recently, we identified two novel virus species within the family *Potyviridae*, *Areca palm necrotic spindle-spot virus* (ANSSV) and *Areca palm necrotic ringspot virus* (ANRSV), which are highly epidemic in main growing regions of areca palm in China, and severely threaten its industrial development (37, 38). ANSSV and ANRSV are closely related and taxonomically classified into a putative new genus (*Arepavirus*) of the family. As a matter of interest, these viruses seem to have a unique pattern of leader proteases formed, apparently, by two HCPro factors (HCPro1 and HCPro2) in tandem. In this study, we experimentally demonstrate that this distinctive pattern is truly encoded by the 5′-terminal region of the ANSSV genome. Further, we found that HCPro1 and HCPro2 have evolved contrasting RNA silencing suppression activity. Eventually, infectivity tests of both wild-type and a series of ANSSV-derived cDNA clones revealed that HCPro1 and HCPro2 might function in a coordinated manner to maintain viral infectivity. The obtained results greatly advance our understanding of the evolution and functional diversification of potyvirids.

RESULTS

Both putative cysteine protease domains in the genomic 5′-terminal region of ANSSV have self-cleavage activity. Previous bioinformatic analysis predicted the presence of two conserved cysteine protease domains of the peptidase_C6 superfamily in the N terminus of ANSSV polyprotein (Fig. 1A). The catalytic activity sites for them were "Gly159, Cys161, and His233" and "Gly461, Cys463, and His535," respectively. Thus, it was speculated that the 5′-terminal region of the ANSSV genome encoded two cysteine proteases in tandem (HCPro1-HCPro2) resulting from *cis*-cleavage at their C terminus (Fig. 1A) (37, 38). To experimentally test the *cis*-cleavage activity of these two domains, a 2,142-nt fragment that corresponds to the 5′-terminal region of the ANSSV genome (HCPro1-HCPro2-P3N cistrons, here named tHCPro-P3N) was introduced into an expression vector, pF3K WG (BYDV) Flexi. An *in vitro* translation assay showed the production of the whole tHCPro-P3N as well as the five expected *cis*-cleavage products (I, II, III, IV, and V), which were absent in the mock control (Fig. 1B and C). Theoretically, a sixth product that represents P3N (∼16.7 kDa) has to be produced; however, it could not be discriminated in the analysis due to strong background signals generated by a wheat germ extract (WGE)-based *in vitro* translation system (Fig. 1C). To further demonstrate the presence of two bona fide cysteine-like proteases in tHCPro-P3N, two mutants were constructed, tHCPro-P3N(C161A) and tHCPro-P3N(C463A), in which the residues C161 and C463 in the expected catalytic sites were mutated by alanine (Fig. 1B). An *in vitro* translation assay showed two major products (I and II) for tHCPro-P3N(C161A) and three bands (I, III, and V) for tHCPro-P3N(C463A) (Fig. 1C), indicating that the mutation of C161 or C463 abolishes the *cis*-cleavage activity of the corresponding cysteine protease domains.

Delineation of HCPro1 and HCPro2 in the ANSSV genome. For potyvirids, the cleavage site of leader cysteine protease is located immediately downstream from the cysteine protease domain, more precisely, at the C terminus of a conserved G residue at the "P1" position of the cleavage site (39). Following these criteria, 258G/V259 and 574G/G575 were initially believed to be the cleavage sites of the two cysteine protease domains of ANSSV, respectively (37, 38). To test this hypothesis, G258A and G574A were engineered into the plasmid that expresses tHCPro-P3N for a further *in vitro* translation assay (Fig. 2A). The results showed that products from tHCPro-P3N(G574A) (Fig. 2B) are equivalent to those from tHCPro-P3N(C463A) (Fig. 1C), indicating that 574G/G575 is
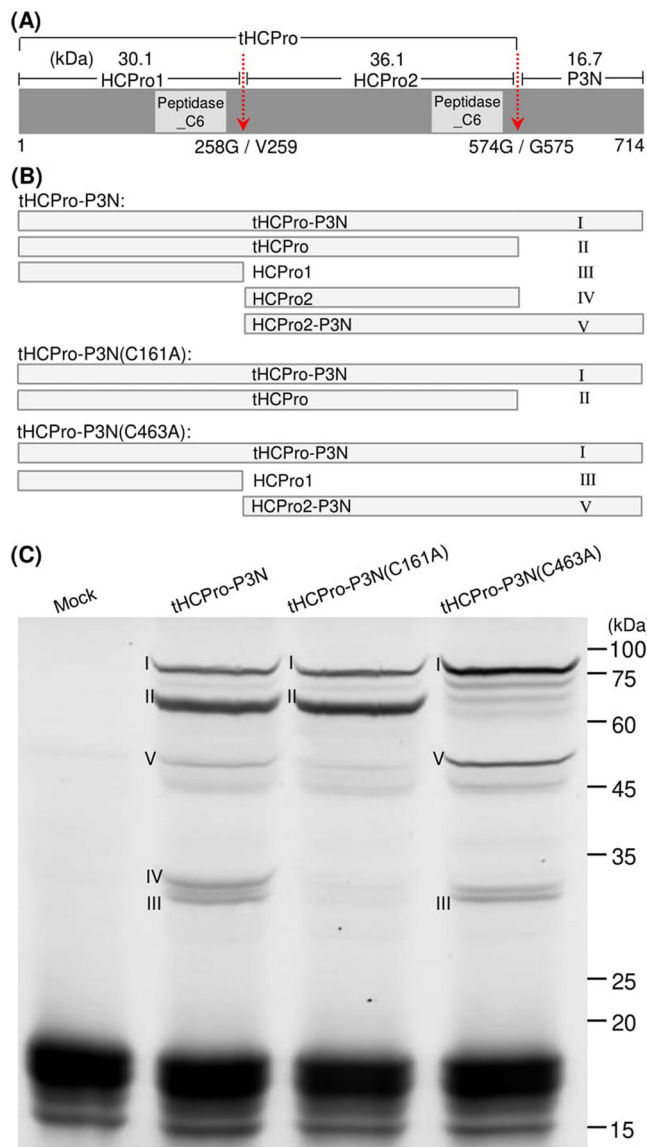
FIG 1 WGE-based *in vitro* translation analysis of tHCPro-P3N and its derivatives, tHCPro-P3N(C161A) and tHCPro-P3N(C463A). (A) Schematic diagram of a 2,142-nt coding region of the genomic N terminus of ANSSV (tHCPro-P3N). Previous bioinformatic analysis predicted the presence of two conserved cysteine protease domains of peptidase_C6 superfamily in the genomic 5'-terminal region of ANSSV (37, 38). After *cis*-cleavage of the two domains, two cysteine proteases (HCPro1 and HCPro2) would be generated. Red arrows indicate the putative cleavage sites of the two cysteine protease domains (37). (B) A predicted profile of products for tHCPro-P3N, tHCPro-P3N(C161A), and HCPro-P3N(C463A) after *in vitro* translation followed by self-cleavage of cysteine protease domains. (C) SDS-PAGE analysis of WGE-based *in vitro* translation products of tHCPro-P3N, tHCPro-P3N(C161A), and tHCPro-P3N(C463A). Mock, empty vector control.

indeed the cleavage site of HCPro2. However, products from tHCPro-P3N(G258A) resulted equivalently to those from the tHCPro-P3N (Fig. 2B), thereby suggesting that 258G/V259 is not the cleavage site of HCPro1. Another suspected cleavage site, 273G/S274, was screened by an *in vitro* translation assay after the introduction of a G273A mutation into the construct that expresses tHCPro1-P3N (Fig. 2A). We found that tHCPro-P3N(G273A) give rise to a profile of products (Fig. 2B) that is equivalent to that of HCPro-P3N(C161A) (Fig. 1C). Therefore, the *cis*-cleavage sites of HCPro1 and HCPro2 were located at position 273G/V274 and 574G/G575, respectively, so that the precise position of these two viral cistrons in the ANSSV genome is delimited (Fig. 2C).
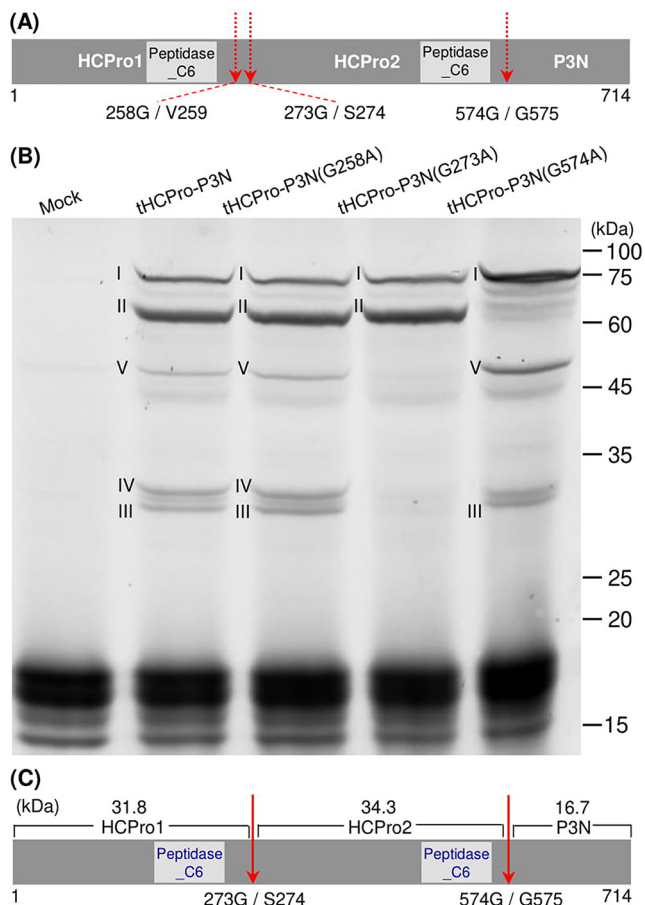
FIG 2 Mapping the *cis*-cleavage sites of the two cysteine protease domains in the 5′-terminal region of ANSSV genome. (A) Schematic diagram of tHCPro-P3N showing two suspected cleavage sites (258G/V259 and 273G/S274) and one site (574G/G575) for the two cysteine protease domains, respectively. The suspected cleavage sites are indicated by dotted arrows. (B) SDS-PAGE analysis of *in vitro* translation products of tHCPro-P3N, tHCPro-P3N(G258A), tHCPro-P3N(G273A), and tHCPro-P3N(G574A). The bands represented by I, II, III, IV, and V are diagrammatically shown in Fig. 1B. Mock, empty vector control. (C) The accurate schematic diagram of the genomic N terminus of ANSSV. The precise *cis*-cleavage sites of the two cysteine protease domains are indicated by red arrows.

Conserved and divergent features of HCPro. For potyvirids, HCPro is one of the most variable proteins (3). In the present study, a comprehensive analysis of 44 representative HCPro sequences distributed into 10 definitive genera and one proposed genus (*Arepavirus*) within the family *Potyviridae* was performed. Multiple sequence alignment revealed that HCPro from most potyvirids (including potyviruses, rymoviruses, roymoviruses, poaceviruses, and ipomoviruses) are longer than 450 amino acids (aa) in size, whereas those of the other four genera (i.e., *Arepavirus*, *Bymovirus*, *Bevemovirus*, and *Macluravirus*) were shorter than 300 aa (Fig. 3 and 4). The significant variation in size of HCPro is mainly attributed to their N-terminal moieties (Fig. 4). Pairwise amino acid sequence comparison revealed that the intergenus similarity of HCPro ranges from 10.5% to 32.1% (data not shown). The corresponding values for cysteine protease domain and N-terminal moiety are 12.9 to ~57.3% and 0 to ~25.4%, respectively (data not shown). Thus, we propose that potyvirid's HCPro factors comprise a variable N-terminal region (N) and a conserved C-terminal cysteine protease domain (D) (Fig. 4).

A phylogenetic analysis of HCPro was performed. Unfortunately, a phylogenetic tree based on full-length HCPro sequences failed to accurately reflect the taxonomic relationship of these virus species (data not shown), presumably due to the high variability at the N region. Thus, phylogenetic analysis based on the D domain was
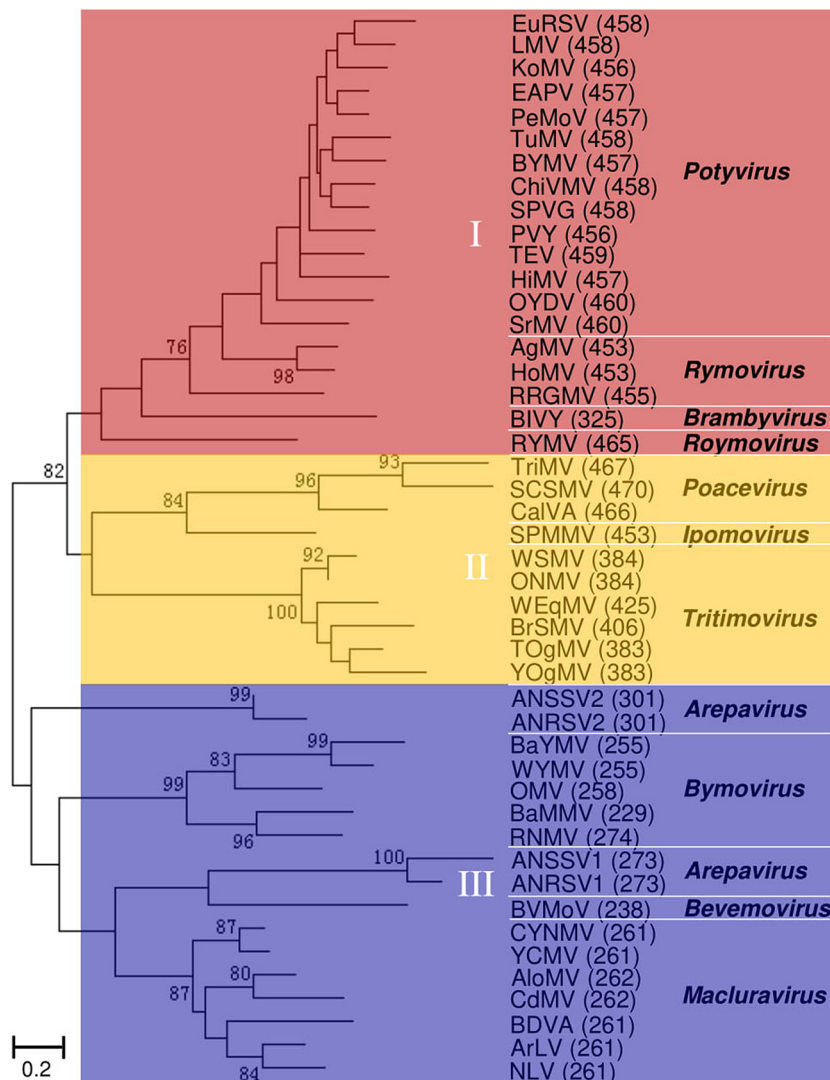
FIG 3 Phylogenetic analysis of the conserved cysteine protease domain of potyvirid HCPros. A total of 44 representative species in 10 definitive and 1 recently proposed genera of the *Potyviridae* family were employed for the phylogenetic analysis. The amino acid sequences of cysteine protease domain of HCPro of these virus species were aligned using ClustalX, and the phylogenetic tree was constructed with MEGA 7.0 using the maximum likelihood method. The numbers at the branch nodes indicate bootstrap support (1,000 replicates). Values below 70% are not shown.

carried out. The result showed that these HCPros can be classified into three groups (named I, II, and III) (Fig. 3). Group I encompasses HCPro factor from four genera (i.e., *Potyvirus*, *Rymovirus*, *Brambyvirus*, and *Roymovirus*). Except for the HCPro from blackberry virus Y (*Brambyvirus* genus) with 326 aa, they have a relatively big size (453 to 466 aa). Importantly, so far, all tested HCPros in group I display RNA silencing suppression activity (5). Group II comprises the HCPro products from three genera, *Poacevirus*, *Ipomovirus*, and *Tritimovirus*. The size of proteins in group II varies greatly, with a range that goes from 384 to 471 aa. Intriguingly, viruses for which HCPro is clustered in group II rely on P1 (type B) rather than HCPro for RNA silencing suppression activity (5). Group III comprises HCPro factors from four genera, *Arepavirus*, *Bymovirus*, *Bevemovirus*, and *Macluravirus*, and they are typically characterized by small HCPros (230 to 301 aa). To date, the functional roles of HCPro belonging to group III have not been defined.

HCPro2 is a viral suppressor of RNA silencing (VSR). Usually, one of the leader proteases of potyvirids executes essential roles in RNA silencing suppression, such as HCPro factor from members of the *Potyvirus* genus (27, 28) and type B P1 protein from

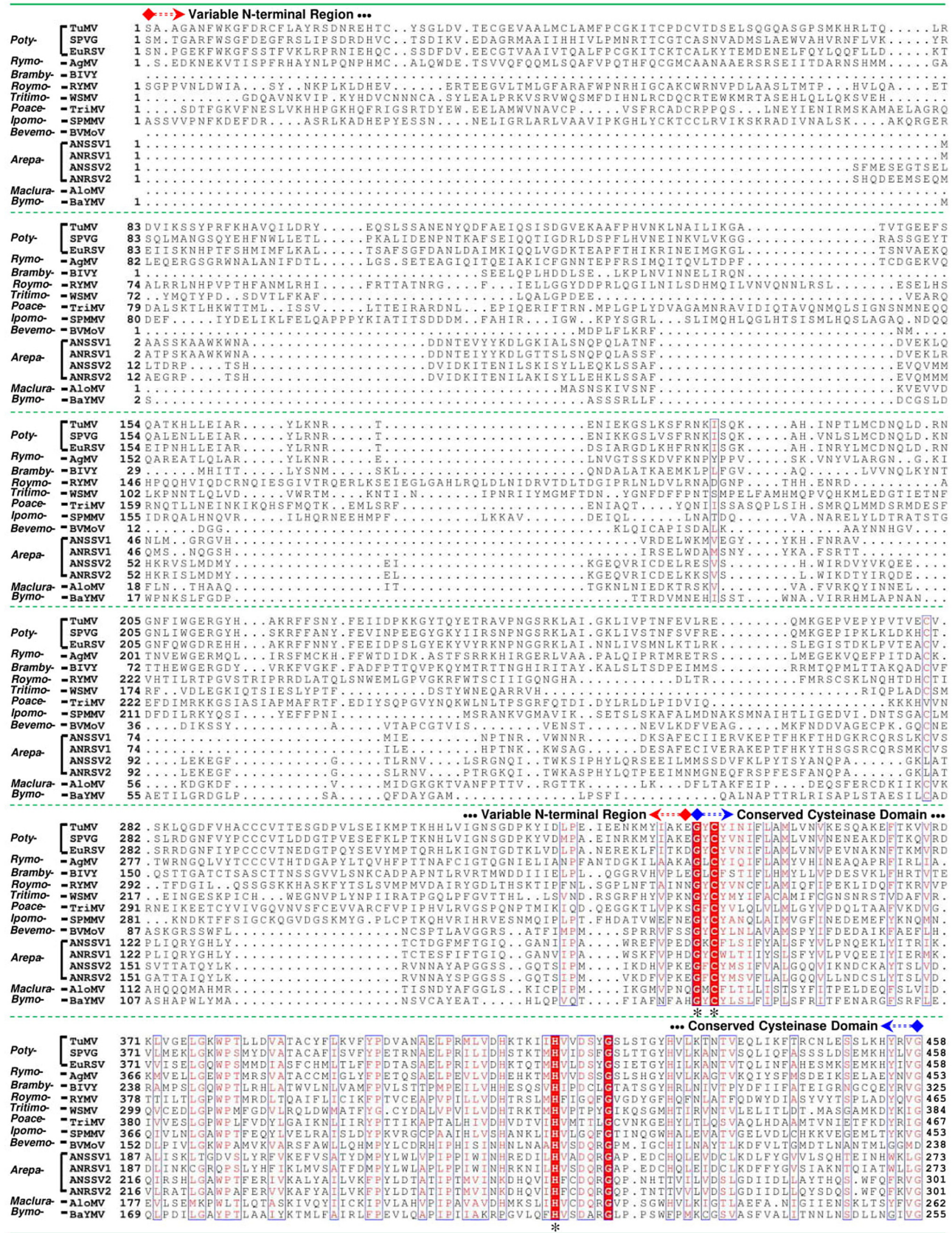FIG 4 Multiple alignment of amino acid sequences of the leader cysteine proteases (HCPro, P2-1, HCPro1, and HCPro2) of 14 representative viruses distributing into 11 genera of the *Potyviridae* family. The variable N-terminal region and conserved cysteine protease domain of the leader cysteine proteases are defined. Three residues, Gly, Cys, and His, as the putative catalytic activity sites, are indicated by asterisks.
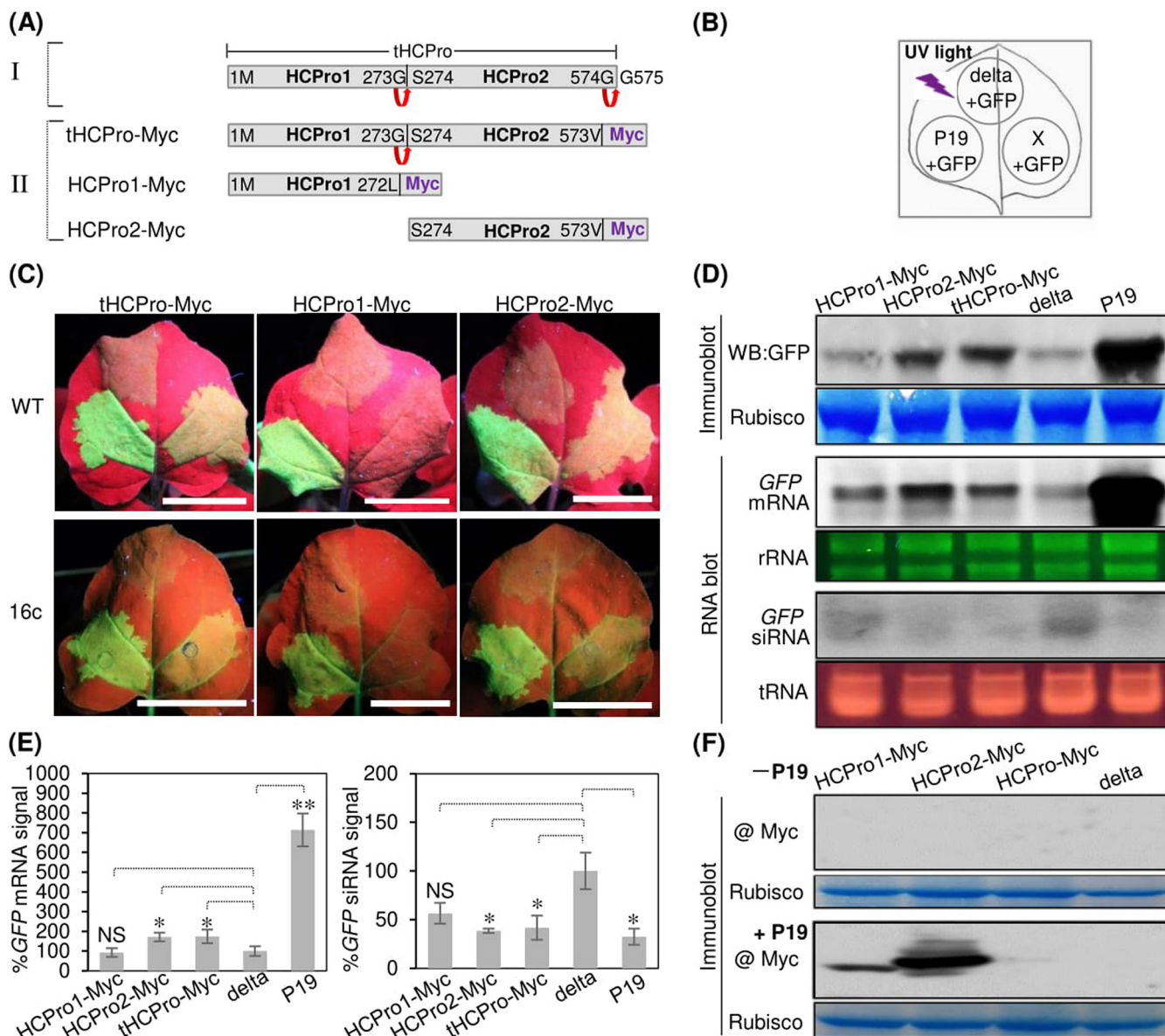
FIG 5 RNA silencing suppression test of tHCPro, HCPro1, and HCPro2 of ANSSV. (A) Schematic diagram of tHCPro-Myc, HCPro1-Myc, or HCPro2-Myc. Diagrams of wild-type tHCPro (I) and its derivatives, tHCPro-Myc, HCPro1-Myc, and HCPro2-Myc (II), are shown. Bent arrows indicate the self-cleavage site of HCPro1 or HCPro2. (B) Patch design used for coinfiltration in wild-type *N. benthamiana* or 16c leaves with a GFP-expressing construct together with a candidate protein-expressing construct (indicated by X), a P19-expressing positive control, or a negative empty vector, pCaMterX control (indicated by delta). (C) Representative photographs of coinfiltrated wild-type *N. benthamiana* (upper) or 16c (lower) leaves taken at 3 dpi under UV light. Bar, 25 mm. (D) Immunoblot and Northern blot analyses of *GFP* silencing in coinfiltrated leaf patches. Coomassie blue staining of the large subunit of rubisco was used as a loading control for the immunoblot. Ethidium bromide (EB) staining of rRNA and tRNA served as the loading controls for Northern blot assays of *GFP* mRNA transcripts and *GFP*-derived siRNAs, respectively. (E) Quantitative analysis of *GFP* mRNA (left) and *GFP*-derived siRNA (right) signals shown in panel D. The signal intensity values are presented as the mean ± standard deviation (SD) ($n = 3$). The average delta values were designated 100% to normalize the data. Statistically significant differences, determined by an unpaired two-tailed Student's *t* test, are indicated by asterisks. *, $P < 0.05$; **, $P < 0.01$; NS, no significant difference. (F) Immunoblot analysis of the transient expression of tHCPro-Myc, HCPro1-Myc, and HCPro2-Myc in *N. benthamiana*; (top) Western blot detection of the expression of tHCPro-Myc, HCPro1-Myc, and HCPro2-Myc; leaf patches indicated in panel B were sampled at 3 dpi; (bottom) Western blot analysis of the expression of tHCPro-Myc, HCPro1-Myc, and HCPro2-Myc. Leaf patches of coinfiltration of TBSV P19, together with tHCPro-Myc, HCPro1-Myc, or HCPro2-Myc, were sampled at 3 dpi for the analysis.

other potyvirids (5). Therefore, the capacity of HCPro1, HCPro2, and tHCPro from ANSSV to counteract the plant-based RNA silencing was investigated. Constructs expressing tHCPro-Myc, HCPro1-Myc, and HCPro2-Myc in plants by agro-infiltration were generated (Fig. 5A) and then introduced in *Agrobacterium tumefaciens*. Each of the generated *A. tumefaciens* strains was later coinfiltrated with another strain that carries a plasmid

that expresses the green fluorescent protein (GFP) reporter into leaves of both wild-type and 16c *Nicotiana benthamiana* plants (Fig. 5B and C). The coinfiltration of GFP along with either empty vector or the silencing suppressor P19 from tobacco bushy stunt virus (TBSV) was included as negative and positive controls, respectively (40, 41) (Fig. 5B and C). At 3 days postinoculation (dpi), leaf patches expressing tHCPro-Myc/GFP or HCPro2-Myc/GFP displayed strong GFP fluorescence (Fig. 5C). No obvious GFP fluorescence was observed on leaf patches expressing HCPro1-Myc/GFP or negative control (Fig. 5C). Western blot analysis showed that the abundance of GFP protein in leaf patches coinfiltrated with tHCPro-Myc/GFP or HCPro2-Myc/GFP was significantly higher than that of HCPro1-Myc/GFP or the negative control (Fig. 5D). Of note, the Northern blot analysis showed that the enhancing levels of GFP expression in the presence of tHCPro-Myc and HCPro2-Myc occur at the level of RNA accumulation. Consequently, a larger amount of *GFP* mRNA transcripts was detected in samples from leaf patches expressing GFP along with either tHCPro-Myc or HCPro2-Myc (Fig. 5D and E). *GFP*-derived small interfering RNAs (siRNAs) were observed as a consequence of *GFP* mRNA silencing in samples from leaf patches expressing most of the constructs. Importantly, these molecules were hardly detectable in samples from leaf patches expressing tHCPro-Myc/GFP, tHCPro2-Myc/GFP, or the P19/GFP positive control (Fig. 5D and E). Remarkably, the expression levels of HCPro1, HCPro2, and tHCPro from above leaf patches were hardly detected by Western blotting assay (Fig. 5F), whereas they were rescued to a varied extent when coinfiltrated with the P19-expressing construct (Fig. 5F). Together, all these data suggest that HCPro2 has RNA silencing suppression activity, whereas HCPro1 does not.

The RNA silencing suppression activity of HCPro2 is independent of its release from the preceding HCPro1. The leader proteases encoded by potyviruses, which are the predominant virus genus of potyvirids, are P1 and HCPro in tandem. As mentioned above, HCPro is the potyviral VSR factor, and its activity depends on its release from the preceding P1 (20, 21, 42). To investigate whether the detachment from HCPro1 is essential for RNA silencing suppression activity of HCPro2, two mutants of tHCPro, tHCPro(C161A) and tHCPro(G273A), in which the *cis*-cleavage activity of HCPro1 was compromised (Fig. 1 and 2), were constructed (Fig. 6A) and subjected to an RNA silencing suppression test. Coexpression with GFP showed that leaf patches expressing tHCPro(C161A)/GFP or tHCPro(G273A)/GFP displayed clear GFP fluorescence, similar to that of leaf patches expressing wild-type tHCPro/GFP (Fig. 6B). In line with this observation, a higher accumulation level of GFP protein and *GFP* mRNA transcript was detected in leaf patches expressing active VSRs but not in the case of the negative control (Fig. 6C and D). Consistently, *GFP*-derived siRNA accumulated significantly more in leaf patches corresponding to the negative control than in those of the other treatments (Fig. 6C and D). These results indicate that the self-cleavage of HCPro1 to release free HCPro2 is not essential for HCPro2-mediated antisilencing activity.

Both N2 and D2 domains of HCPro2 confer RNA silencing suppression activity independently. To determine the domain(s) of HCPro2 that confer(s) antisilencing activity, two constructs that transiently express N2 and D2 of HCPro2, respectively, were constructed (Fig. 7A). Transient coexpression experiments showed that leaf patches corresponding to N2/GFP and D2/GFP, similar to those of HCPro2/GFP, displayed strong GFP fluorescence (Fig. 7B). Consistently, Western blot analysis revealed that the abundance of GFP protein in leaf patches expressing N2/GFP, D2/GFP, and HCPro2/GFP was significantly higher than that of the negative control (Fig. 7C). Supporting the above-described conclusion, a higher accumulation level of *GFP* mRNA transcripts in leaf patches expressing N2/GFP, D2/GFP, and HCPro2/GFP than that of the negative control was observed (Fig. 7C and D).

The HCPro1 D1 domain prevents the RNA silencing suppression activity of the whole HCPro1 protein. Given that the cysteine protease domains of HCPro1 and HCPro2 are conserved (Fig. 4) and that HCPro2 D2 has antisilencing activity, we wondered whether the conserved cysteine protease domain of HCPro1 (D1) has RNA silencing suppression activity. We constructed two plasmids to express N1 or D1
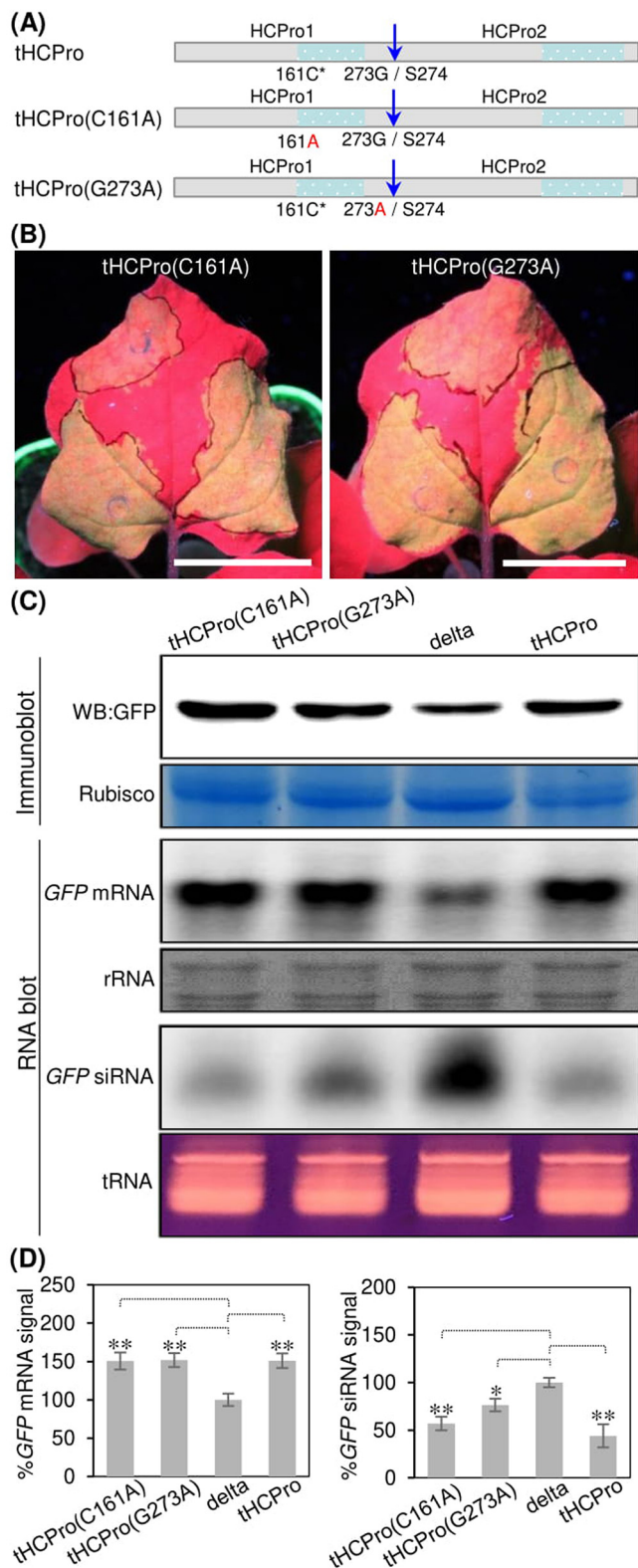
FIG 6 The inactivation of the self-cleavage of HCPro1 has no influence on the antisilencing activity of HCPro2. (A) Schematic diagram of wild-type tHCPro and its derivatives, tHCPro(C161A) and tHCPro(G273A). The shaded regions in blue represent the cysteine protease domain of HCPro1 and HCPro2. The *cis*-cleavage sites of the cysteine protease domains are indicated by blue arrows. (B) Representative photographs of coinfiltrated *N. benthamiana* leaves taken at 3 dpi under UV light. Patch distribution for coinfiltration is exactly the same as that shown in Fig. 5B, except that tHCPro-expressing construct serves as a positive control. Bar, 25 mm. (C) Immunoblot and Northern blot analyses of *GFP*

domains of HCPro1 separately (Fig. 7A). Surprisingly, a coinfiltration experiment showed that leaf patches producing N1/GFP, but not D1/GFP, displayed strong GFP fluorescence (Fig. 7B), indicating that the variable N-terminal region rather than the conserved cysteine protease domain from HCPro1 has RNA silencing suppression activity. Detection of GFP by Western blotting, as well as detection of *GFP* mRNA transcripts by Northern blotting confirmed the above-described result (Fig. 7C and D). Since the whole HCPro1 lacks RNA silencing suppression activity (Fig. 5), we speculated that the conserved cysteine protease domain of HCPro1 might repress the antisilencing activity of the HCPro1 N1 domain. To test this idea, we swapped the protease domain of HCPro1 and HCPro2 to generate two chimeras: N1-D2 and N2-D1 (Fig. 8A), and then carried out an RNA silencing suppression test. Similar to the positive control that expresses HCPro2/GFP, leaf patches corresponding to N1-D2 displayed strong GFP fluorescence signals (Fig. 8B). However, similar background fluorescence was observed in leaf patches of N2-D1/GFP and the negative control (Fig. 8B). As expected, Western blot analysis of GFP and Northern blot detection of *GFP* mRNA transcripts supported the above-described conclusion (Fig. 8C and D). These results suggest that the C-terminal cysteine protease domain of HCPro1 is a genuine regulator of the N-terminal domain-mediated silencing suppression.

Development of ANSSV-derived full-length infectious cDNA clones. Conventional cloning technologies were adopted to construct the complete cDNA clone of ANSSV-HNBT with the low-copy mini-binary T-DNA vector pCB301-35S-Nos (43) as the backbone. The entire genomic cDNA of ANSSV-HNBT was placed between the 35S promoter and Nos terminator in pCB301 to generate the complete cDNA clone of ANSSV (named pSS-I) (Fig. 9A and B). For pSS-I, a 220-bp intron 2 of the *NiR* gene of *Phaseolus vulgaris* was inserted into the P3-coding region of the ANSSV genome in order to attenuate the toxicity of this region in *Escherichia coli* (Fig. 9A). To test the infectivity of pSS-I, 10 *N. benthamiana* seedlings at 6- to 7-leaf stage were infiltrated with an *A. tumefaciens* strain that harbors this plasmid. At 25 dpi, the newly emerging leaves of all plants infiltrated with pSS-I showed vein-clearing symptoms, which were absent in the mock control (Fig. 9C). Typical symptoms of viral infection, such as foliar chlorosis and leaf distortion, were observed in systemic leaves at 35 dpi (Fig. 9C). The presence of ANSSV was confirmed by reverse transcriptase PCR (RT-PCR) amplification of CP- and P3-derived fragments (Fig. 9C). As expected, Sanger sequencing of the PCR products demonstrated that the intron sequence in P3 was completely spliced out from the viral progeny (Fig. 9C).

To create a GFP-tagged version of ANSSV, the GFP cistron was integrated into the NIb/CP intercistronic junction in pSS-I to build the clone pSS-I-G (Fig. 9B). To examine the infectivity of pSS-I-G, eight *N. benthamiana* plants (6- to 7-leaf stage) were inoculated with an *A. tumefaciens* strain that carries pSS-I-G, and then GFP fluorescence signals were recorded at different time points. At 30 dpi, strong fluorescence signals were observed for all infiltrated plants under a UV lamp at the veins of upper noninoculated leaves (Fig. 9D). The stable presence of foreign GFP cistron in the ANSSV genome of the virus progeny was confirmed by RT-PCR (Fig. 9D). Furthermore, GFP production in systemically infected tissues was confirmed by Western blotting analysis. A major band corresponding to the predicted size for the recombinant GFP (approximately 27.8 kDa) was detected, indicating that free GFP protein was efficiently processed and released from the virus genome-encoded polyprotein (Fig. 9D).

FIG 6 Legend (Continued)
silencing in coinfiltrated leaf patches. Coomassie blue staining of the large subunit of rubisco was used as a loading control for the immunoblot. EB staining of rRNA and tRNA served as the loading controls for Northern blot assays of *GFP* mRNA transcripts and *GFP*-derived siRNAs, respectively. Delta, an empty vector control (pCaMterX/35S:GFP). (D) Quantitative analysis of *GFP* mRNA (left) and *GFP*-derived siRNA (right) signals shown in panel C. The signal intensity values are presented as mean ± SD ($n = 3$). The average delta values were designated 100% to normalize the data. Statistically significant differences, determined by an unpaired two-tailed Student's *t* test, are indicated by asterisks: *, $P < 0.05$; **, $P < 0.01$.
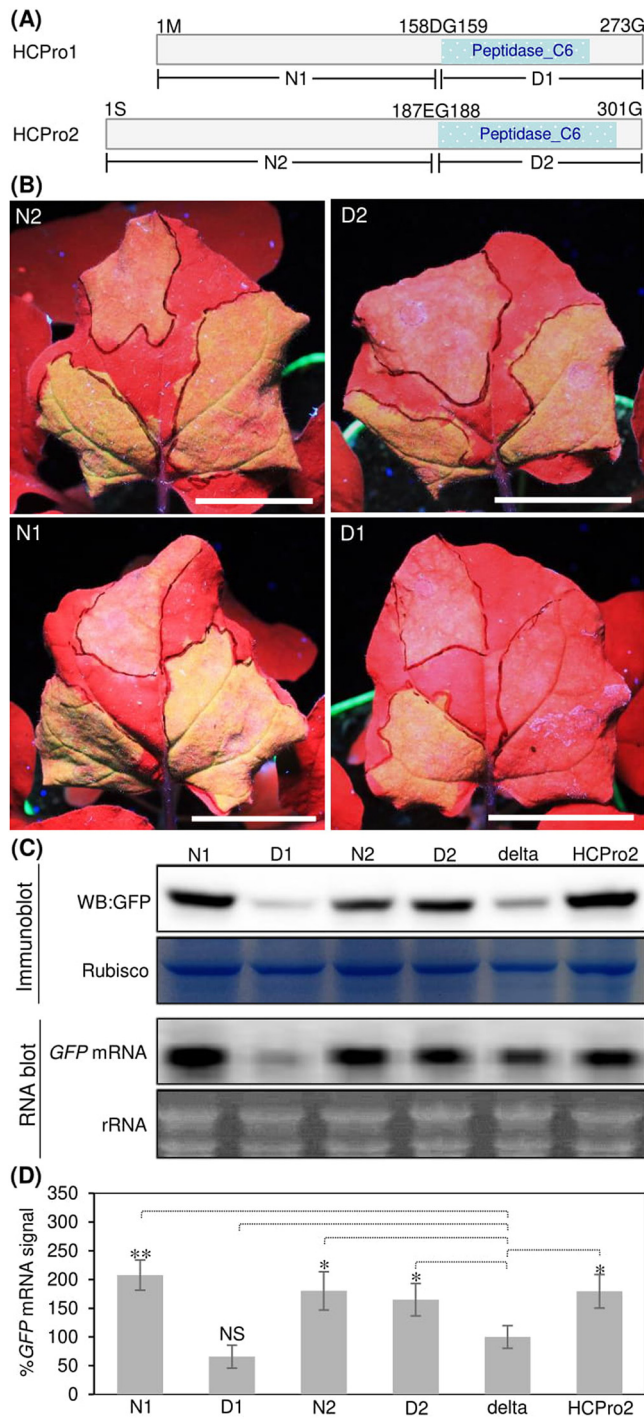
FIG 7 RNA silencing suppression test of the variable N-terminal region (N) and conserved C-terminal cysteine protease domain (D) of HCPro1 and HCPro2. (A) Schematic diagram of HCPro1 and HCPro2 showing the N and D domains. (B) Representative photographs of coinfiltrated *N. benthamiana* leaves at 3 dpi under UV light. Patch distribution for coinfiltration is exactly the same as that shown in Fig. 5B, except that the HCPro2-expressing construct served as a positive control. Bar, 25 mm. (C) Immunoblot and Northern blot analyses of *GFP* silencing in coinfiltrated leaf patches. Coomassie blue staining of the large subunit of rubisco was used as a loading control for the immunoblot. EB staining of rRNA served as the loading controls for Northern blot assays of *GFP* mRNA transcripts. Delta, an empty vector control (pCaMterX/35S:GFP). (D) Quantitative analysis of *GFP* mRNA signals shown in panel C. The signal intensity values are presented as the mean $\pm$ SD ($n = 3$). The average delta value was designated 100% to normalize the data. Statistically significant differences, determined by an unpaired two-tailed Student's *t* test, are indicated by asterisks. *, $P < 0.05$; **, $P < 0.01$; NS, no significant difference.

FIG 8 RNA silencing suppression test of two chimeras (N1-D2 and N2-D1). (A) Schematic diagram of two hybrids (N1-D2 and N2-D1) that were generated by swapping the D domain of HCPro1 and HCPro2. (B) Representative photographs of coinfiltrated *N. benthamiana* leaves at 3 dpi under UV light. The patch design for coinfiltration is exactly the same as that shown in Fig. 5B, except that the HCPro2-expressing construct is served as a positive control. Bar, 25 mm. (C) Immunoblot and Northern blot analyses of *GFP* gene silencing in coinfiltrated leaf patches. Coomassie blue staining of the large subunit of rubisco was used as a loading control for the immunoblot. EB staining of rRNA served as the loading controls for Northern blot assays of *GFP* mRNA transcripts. Delta, an empty vector control (pCaMterX/35S:GFP). (D) Quantitative analysis of *GFP* mRNA signals shown in panel C. The signal intensity values are presented as the mean $\pm$ SD ($n = 3$). The average delta value was designated 100% to normalize the data. Statistically significant differences, determined by an unpaired two-tailed Student's *t* test, are indicated by asterisks. *, $P < 0.05$; ***, $P < 0.001$; NS, no significant difference.
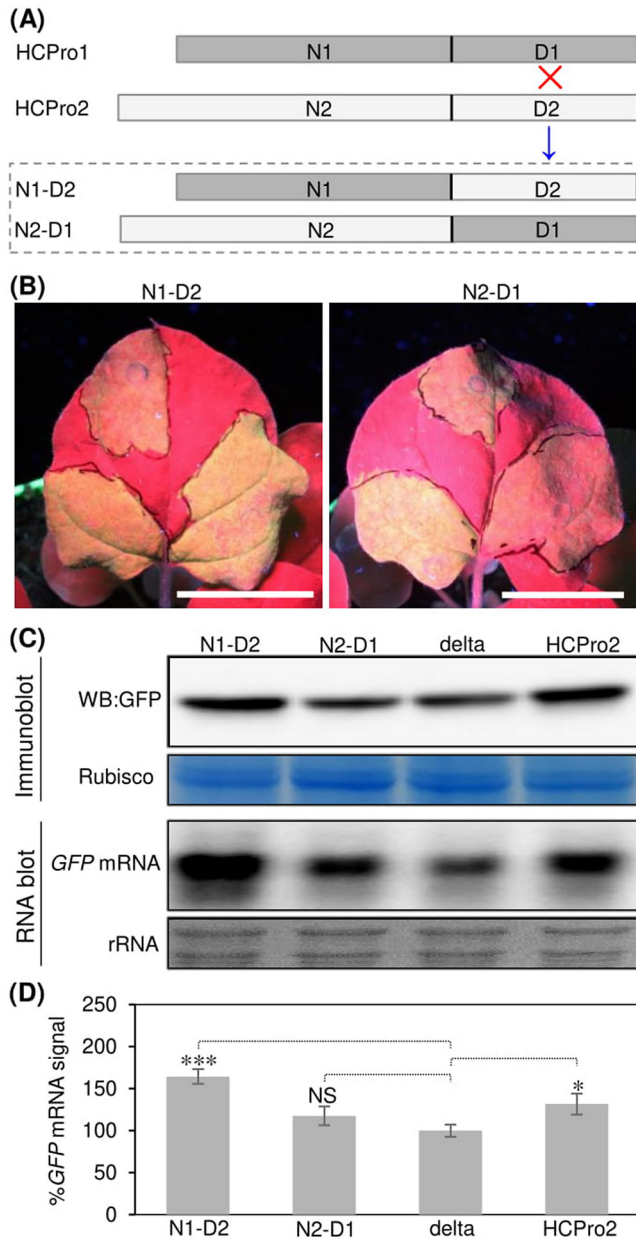
Deletion of either HCPro1 or HCPro2 prevents systemic infection of the resulting ANSSV mutants, and neither of them can be functionally replaced, respectively, by the P1 and HCPro of a potyvirus (TuMV). To test the importance of HCPro1 and HCPro2 during the viral infection cycle, two ANSSV-derived cDNA clones, termed pSS-I-G(Δ1) and pSS-I-G(Δ2), in which the complete HCPro1- or HCPro2-coding region
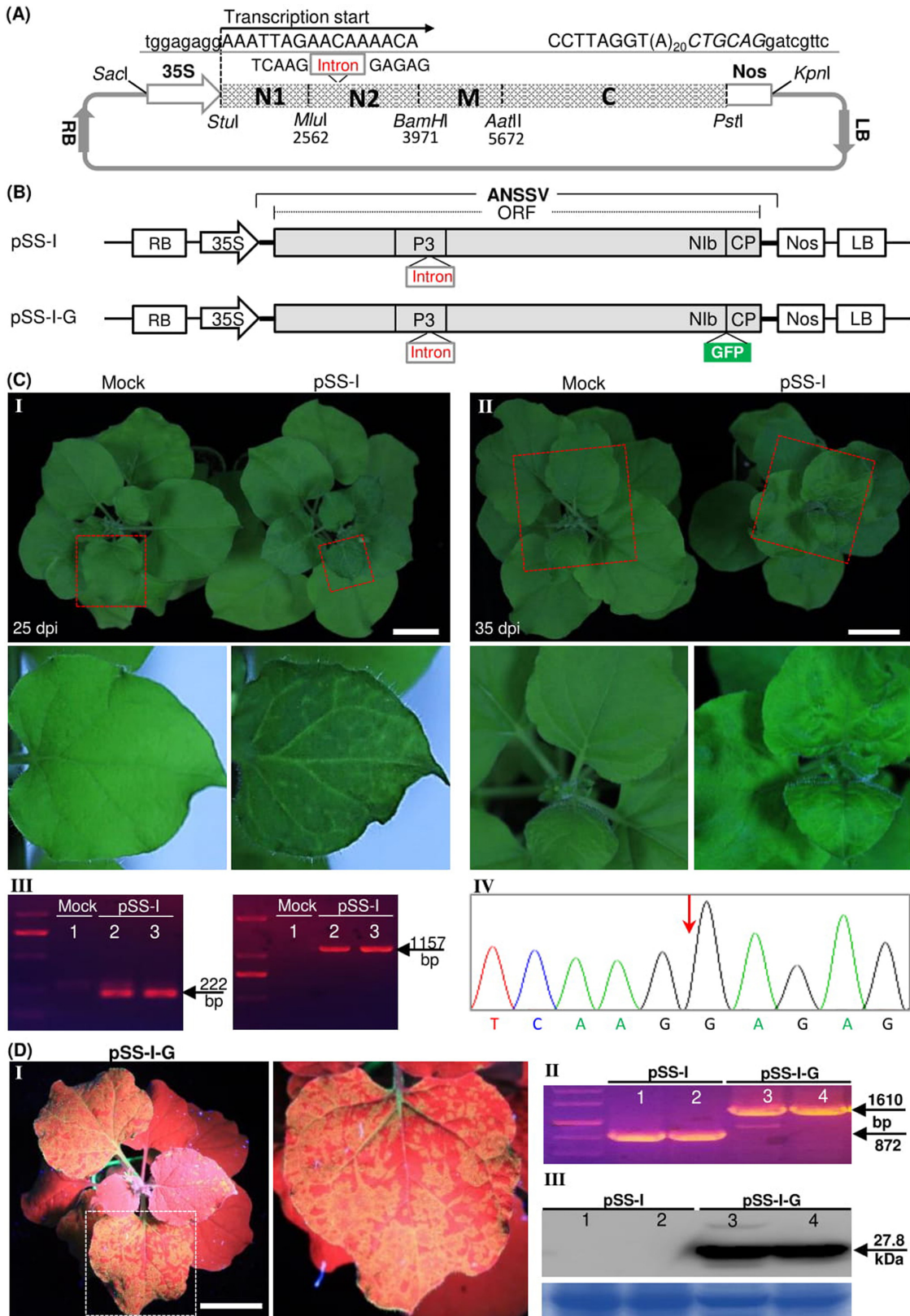
FIG 9 The infectivity test of ANSSV-derived cDNA clones. (A) T-DNA construct representing the complete cDNA clone of ANSSV (pSS-I). The entire genomic cDNA of ANSSV (from the 5′ terminus: N1, N2, M, and C) harboring an intron in the P3-coding region was placed between the 35S promoter and the Nos terminator of mini-binary plant expression vector pCB301-35S-Nos (43). The intron (indicated by a short rectangular box) and its flanking P3-coding sequences are shown. The transcription start site is indicated by a bent arrow. Nucleotides belonging to the pCB301 backbone are indicated in lowercase. Viral nucleotides are indicated in uppercase. The PstI site

was deleted, were constructed (Fig. 10A). At 30 dpi, obvious GFP fluorescence was observed in upper noninoculated leaves, flowers, and stems of all plants inoculated with wild-type pSS-I-G. In contrast, the GFP fluorescence was absent in plants inoculated with either pSS-I-G(Δ1) or pSS-I-G(Δ2) (Fig. 10B). These plants were sequentially monitored until 60 dpi with equivalent observations (data not shown). Both RT-PCR and Western blot assays confirmed the presence of the recombinant virus in upper noninoculated leaves of plants infected with pSS-I-G but not in those inoculated with pSS-I-G(Δ1) or pSS-I-G(Δ2) (Fig. 10C). Altogether, these results suggest that both the HCPro1- and HCPro2-coding regions are indispensable for viral infection.

Potyviruses (members of the genus *Potyvirus*), the predominant and well-studied virus species within the family *Potyviridae*, encode leader serine and cysteine proteases (P1-HCPro) in tandem, such as a 362-aa P1 and 458-aa HCPro for turnip mosaic virus (TuMV). Potyviral P1 plays multiple accessory roles during the viral infection cycle (44–47), but it seems to be unnecessary for viral systemic infection (20, 42). Potyviral HCPro is the VSR factor, which could be replaced by other heterologous VSRs to support viral systemic infection (48, 49). Unlike the leader proteases P1 and HCPro that potyviruses possess, ANSSV belonging to another genus (*Arepavirus*) has, instead, an HCPro1 and HCPro2 of 273 and 301 aa in length, respectively (Fig. 3 and 4). To further dissect additional functions of HCPro1 or HCPro2 during infection, we built two chimeric clones, pSS-I-G(P1) and pSS-I-G(HCPro), in which either HCPro1 or HCPro2 of ANSSV was substituted by the corresponding counterparts, P1 or HCPro from TuMV, respectively (Fig. 10A). *N. benthamiana* plants inoculated with pSS-I-G(P1) or pSS-I-G(HCPro) did not display GFP fluorescence in upper noninoculated leaves at 30 dpi (Fig. 10B). Further, two more hybrid viruses, pSS-I-G(P1HCPro) and pCBTuMV(HCPro1/2), were created via swapping the complete HCPro1-HCPro2 of ANSSV and P1-HCPro of TuMV (Fig. 10A). Similar to pSS-I-G(P1) and pSS-I-G(HCPro), pSS-I-G(P1HCPro) compromised viral infectivity (Fig. 10D). Surprisingly, the HCPro1-HCPro2 of ANSSV that has RNA silencing suppression activity was unable to replace the P1-HCPro of TuMV to maintain viral infectivity for pCBTuMV(HCPro1/2) (Fig. 10D), indicating that the unique TuMV P1-HCPro might function in other essential step(s) in viral infection beyond RNA silencing suppression. The above-described results were confirmed by RT-PCR and/or Western blot assays (Fig. 10C and E). All in all, replacement of HCPro1 or/and HCPro2 in ANSSV by the corresponding counterparts of a heterologous potyvirus has a deleterious effect, suggesting that HCPro1 and HCPro2 function in a coordinated manner to maintain viral infection.

DISCUSSION

In summary, this study with ANSSV experimentally demonstrates for the first time the presence of a unique pattern of leader proteases formed by HCPro1 and HCPro2 in tandem in a member of the family *Potyviridae*, which is the most important group of viruses infecting plants with RNA genomes. Interestingly, whereas HCPro1 and HCPro2 are closely related (Fig. 4), they greatly differ from their counterparts in other potyvirids when comparing sizes and amino acid composition (Fig. 4; data not shown). Despite their similarity, these two leader cysteine proteases are divergent in terms of their

FIG 9 Legend (Continued)

is shown in italicized uppercase. 35S, the cauliflower mosaic virus 35S promoter; Nos, the nopaline synthase terminator; LB, left border; RB, right border. (B) Schematic representation of pSS-I and pSS-I-G. For pSS-I-G, the GFP-coding sequence was integrated into the NIb/CP junction of ANSSV. (C) Infectivity test of pSS-I in *N. benthamiana*. The representative photographs of agro-infiltrated plants were taken at 25 dpi (panel I) and 35 dpi (panel II). Bar, 25 mm. The close view of leaf regions (indicated by red box) is shown. Mock, empty vector control. The presence of ANSSV was detected by RT-PCR to target its CP- (left) and P3-derived (right) fragments (III). Sanger sequencing revealed the intron sequence was completely spliced from virus progeny of the pSS-I clone (IV). The red arrow indicated the insertion site of the intron in pSS-I-G. (D) Infectivity test of pSS-I-G in *N. benthamiana*. The representative photograph of plants infiltrated with pSS-I-G are taken at 30 dpi under UV light (I). The close view of the leaf region (indicated by white box) is shown. Bar, 3 cm. RT-PCR with a pair of primers analyzed the presence of the GFP cistron in virus progeny derived from the pSS-I-G clone (II). The two primers were positioned upstream and downstream, respectively, of the GFP-coding region in pSS-I-G. Western blot detection of GFP in infected *N. benthamiana* plants at 30 dpi (III). Arrow, free GFP (~27.8 kDa). A Coomassie brilliant blue-stained gel was used as a loading control.
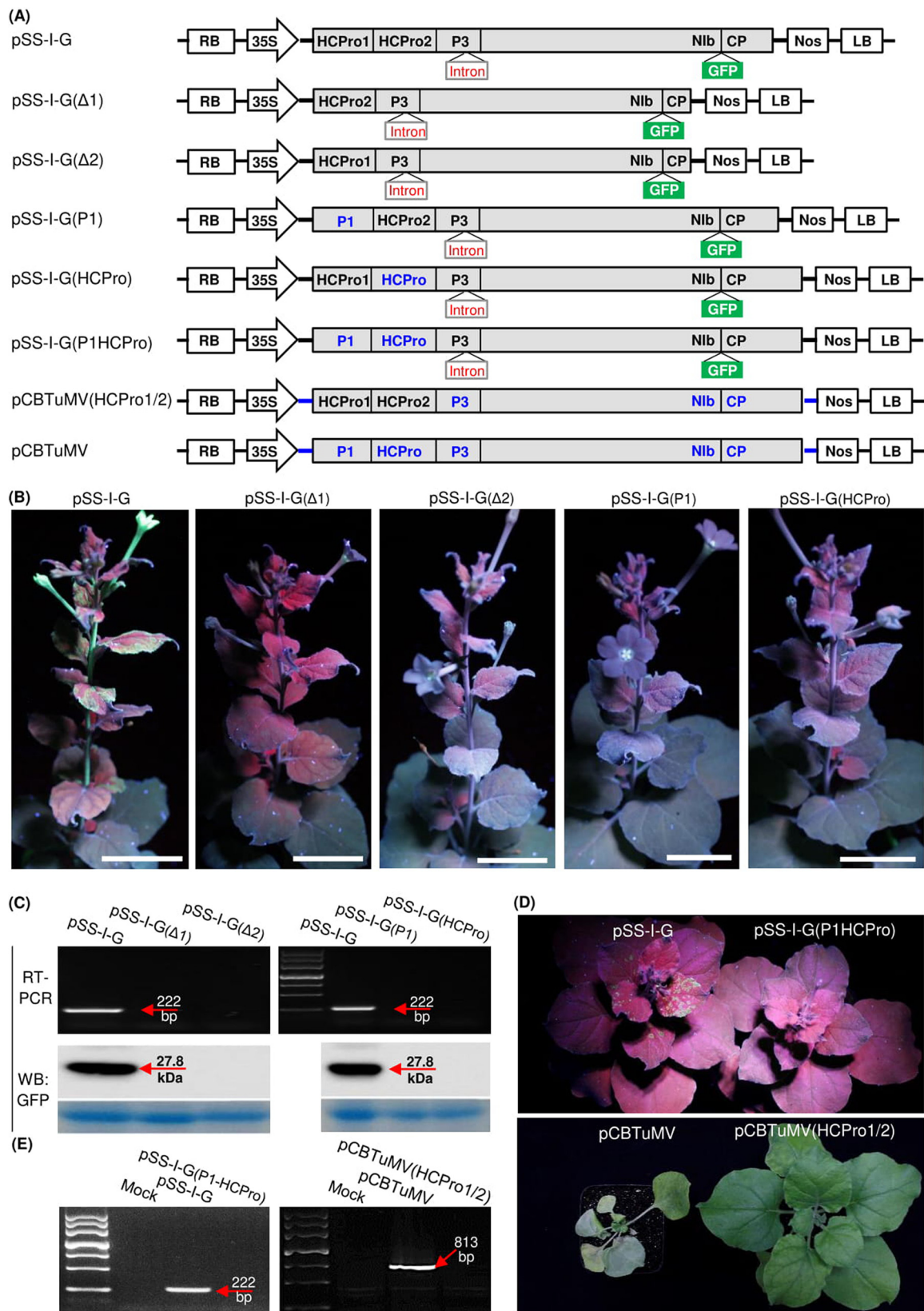
FIG 10 The infectivity test of two ANSSV deletion mutants, as well as four hybrid viruses between ANSSV and TuMV. (A) Schematic diagram of T-DNA constructs representing different viral clones. (B) Infectivity test of pSS-I-G(Δ1), pSS-I-G(Δ2), pSS-I-G(P1), and pSS-I-G(HCPro) in *N. benthamiana*. Ten seedlings at the 6- to 8- leaf stage were agroinfiltrated with each construct. The representative photographs of agro-infiltrated plants were taken at 30 dpi under UV light. Bar, 5 cm. (C) RT-PCR detection and/or Western blot assay of

(Continued on next page)

capacity to block RNA silencing, an evolutionarily conserved and sequence-specific immune response against viral infections in plants and other eukaryotes (33, 34, 50, 51). Our results also suggest that (i) HCPro1 and HCPro2 are indispensable for viral compatible infection and (ii) HCPro2 has, apart from RNA silencing suppression activity, additional essential functions that cannot be replaced by a heterologous VSR.

The potyviral HCPro is a well-studied VSR. It works mainly by direct interaction with, and sequestration of, vsiRNAs as well as, apparently, via interference with diverse steps of the RNA silencing machinery (3, 5, 52–56). Although both HCPro1 and HCPro2 from ANSSV do not have the well-conserved, antisilencing-related FRNK motif at their central regions (3), HCPro2 is a potent VSR, and HCPro1 does the same when its C-terminal part is deleted. Therefore, we envisage a scenario in which HCPro2 (and the N terminus of HCPro1) uses a different strategy than potyviral HCPro to block RNA silencing. Indeed, HCPro2 behaves differently than its potyviral counterpart, as both its variable N-terminal region and conserved C-terminal cysteine protease work as VSRs independently (Fig. 7). Moreover, whereas the potyviral HCPro becomes active after its release from the upstream protease P1 (20, 21, 57), the ANSSV HCPro2 silencing suppression activity is independent of the release from its upstream protease HCPro1. Intriguingly, potyviral P1 is dispensable for viral viability (20, 42), while HCPro1, the counterpart in ANSSV, is indispensable (Fig. 10). From now on, our further efforts will be focused on unraveling (i) the meaning of these differences between arepaviruses and potyviruses and, of course, (ii) the molecular mechanism by which HCPro1 and HCPro2 from ANSSV act coordinately to interfere with antiviral silencing.

Several Western blot assays failed to detect the expression level of HCPro1, HCPro2, and tHCPro from the corresponding coinfiltrated leaf patches (Fig. 5F). Therefore, we performed a coinfiltration assay of HCPro1, HCPro2, or tHCPro, together with a P19-expressing construct. It was found that the accumulation of HCPro2 was significantly increased (Fig. 5F), possibly implying a certain counter-counter-defense response deployed by host cells. Still, the expression of HCPro1 and the HCPro2 released from the precursor tHCPro was largely unrescued (Fig. 5F). Based on this, we propose that some cellular degradation machinery, such as selective autophagy and/or ubiquitin-proteasome (34, 41, 58–60), might be involved in the degradation of HCPro1 as well as HCPro2 when the last is expressed attached to the first. Therefore, further dissection on the molecular mechanism underlying the degradation of HCPro1 and its complex relationship with HCPro2 remains to be investigated.

For potyviruses, deletion of the whole HCPro or the introduction of point mutations abolishing HCPro-mediated silencing suppression generates a defective virus that is no longer able to initiate an infection (61). However, as in the case of PPV, the replacement of HCPro (or P1-HCPro) by other heterologous VSRs generates viable viruses able to reach upper noninoculated leaves with different efficiencies (48, 49, 62). Unlike PPV, the chimeric ANSSV clone, which was generated via replacement of HCPro2 (or HCPro1-HCPro2) by the potent VSR HCPro (or P1-HCPro) from TuMV, is unable to even initiate infection in *N. benthamiana* (Fig. 10), suggesting that HCPro2 plays other essential function(s), apart from RNA silencing suppression, during the viral infection cycle. It has to be mentioned that the complete P1-HCPro of TuMV is unable to be substituted by HCPro1-HCPro2 of ANSSV that has RNA silencing suppression activity to support viral infection (Fig. 10). This seems to be contradictory to previous observations of the well-studied PPV (48, 49, 62). It is noted that the hypervariable leader proteases of different potyvirids (even among viruses in the same genus) (5) might play multiple

FIG 10 Legend (Continued)

viral infection in *N. benthamiana* plants inoculated with the indicated constructs. The newly expanded leaves of inoculated plants were sampled at 30 dpi. (D) Infectivity test of pSS-I-G(P1HCPro) and pCBTuMV(HCPro1/2) in *N. benthamiana*. Ten seedlings at the 6- to 8- leaf stage were agroinfiltrated with each construct. For pSS-I-G and pSS-I-G(P1HCPro), the representative photographs of inoculated plants were taken at 30 dpi (under UV lamp), and for pCBTuMV and pCBTuMV(HCPro1/2), at 14 dpi. (E) RT-PCR detection of viral infection in *N. benthamiana* plants agroinfiltrated with the indicated constructs. For pSS-I-G and pSS-I-G(P1HCPro), the newly expanded leaves of inoculated seedlings were assayed at 30 dpi, and for pCBTuMV and pCBTuMV(HCPro1/2), at 14 dpi. Arrow, free GFP (~27.8 kDa). A Coomassie brilliant blue-stained gel was used as a loading control.
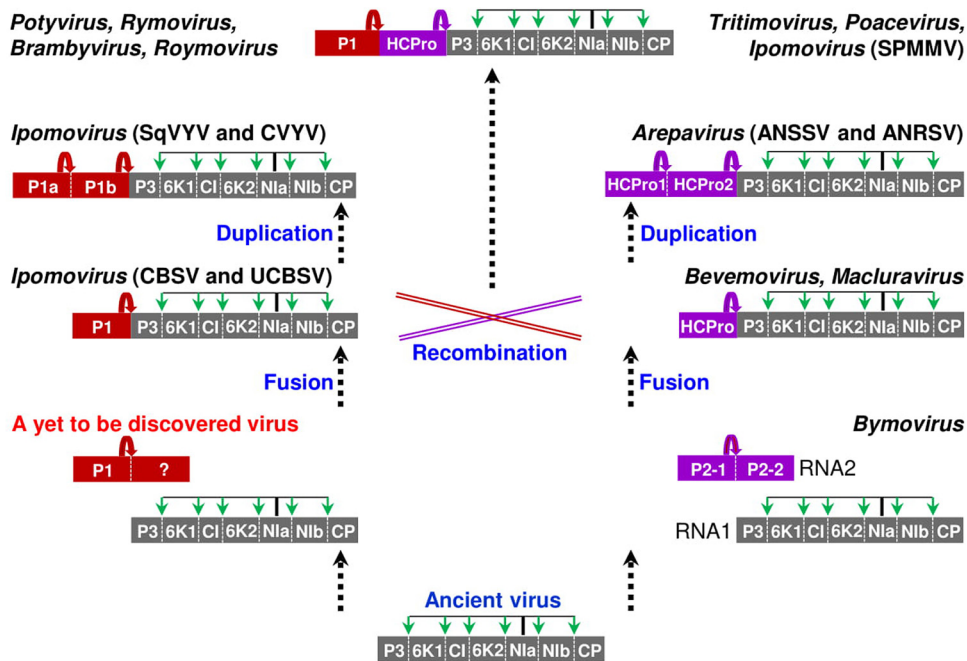
FIG 11 A proposed model that reflects an evolutionary relationship of viruses in the *Potyviridae* family. The conserved region starting from P3 through CP is proposed to be a basic module for two separate evolutionary lineages. Two separate evolutionary lineages would be expanded along the basic module. A recombination event might occur between the single P1-typed ipomovirus and HCPro-typed bevemovirus/macluravirus for the origin of virus species with leader P1 and HCPro. SqVYV, *Squash vein yellowing virus*; CVYV, *Cucumber vein yellowing virus*; CBSV, *Cassava brown streak virus*; UCBSV, *Uganda cassava brown streak virus*.

(but not exactly the same) essential roles in successful viral infection. For instance, apart from RNA silencing suppression activity, potato virus A (a member of the *Potyvirus* genus) HCPro promotes viral genome translation via inducing the formation of RNA granules (63, 64). This will be a fascinating and promising research direction in the future. Nevertheless, it remains to be determined whether all these mutant viruses generated in this study that fail to be systemic infections have defects in the infection of the inoculated leaves.

Based on the results presented here, we built a simplified model that might reflect the evolution of potyvirids (Fig. 11). It is logical to think that the conserved region from P3 to CP, which is proteolytically processed by the viral-encoded NIa-Pro, is the most ancient and basic viral module (3). Two separate lineages would have evolved from that (Fig. 11). One lineage corresponds to some ipomoviruses which harbor a single leader P1, possibly by acquiring P1 into the basic module. Although the genesis of the P1 element has not been determined, we attempt to speculate that an undiscovered virus that has a bi-segmented genome similar to that of bymoviruses might serve as a donor of P1 (Fig. 11). Later, with a putative duplication of P1, other ipomoviruses evolved two P1s in tandem (P1a and P1b). The other lineage might have evolved bevemoviruses and macluraviruses, in which the basic module incorporated a single leader HCPro of small size likely from RNA-2 of bymoviruses. A duplication of HCPro would have generated ANSSV and ANRSV arepaviruses with a distinct pattern of leader proteases: HCPro1 and HCPro2 in tandem. Finally, a recombination event might have occurred between the single P1-typed ipomovirus and HCPro-typed bevemovirus/macluravirus, giving rise to the most widespread potyvirid species, which have P1 and HCPro as leader proteases (Fig. 11). All in all, the study presented here with an arepavirus fills a missing piece in the evolutionary path of viruses in the *Potyviridae* family.

MATERIALS AND METHODS

Viral isolate and plant materials. In this study, an ANSSV isolate HNBT, whose genome was completely determined (GenBank accession no. MH330686) (37), was subjected to construction of the

indicated plasmids as well as generation of ANSSV-derived infectious cDNA clones. The seedlings of wild-type *N. benthamiana* or the green fluorescent protein gene (*GFP*)-transgenic line (16c) were maintained in a growth chamber with 16 h of light at 25°C and 8 h of darkness at 23°C.

Plasmid construction. To detect two putative cysteine protease domains in the presence of the N terminus of ANSSV polyprotein, a 2,142-nt coding region that corresponds to the genomic 5′-terminal region of ANSSV (tHCPro-P3N) was amplified by RT-PCR. The resulting product was integrated into pF3K WG (BYDV) Flexi (Promega) by AsiSI/PmeI sites to generate plasmid pF3-tHCPro-P3N. Two derivatives of pF3-tHCPro-P3N, pF3-tHCPro-P3N(C161A) and pF3-tHCPro-P3N(C463A), in which the residues C161 and C463 in catalytic activity sites were, respectively, mutated into alanine, were constructed using the overlapping PCR method. To map the *cis*-cleavage sites of HCPro1 and HCPro2, the other three mutants, pF3-tHCPro(G258A), pF3-tHCPro(G273A), and pF3-tHCPro(G574A), in which the residues G258 and G273 at the "P1" position of two suspected *cis*-cleavage sites of HCPro1 and the residue G574 of HCPro2 were, respectively, mutated into alanine, were created.

For RNA silencing suppression assays, we constructed three plasmids (pCaM-tHCPro-Myc, pCaM-HCPro1-Myc, and pCaM-HCPro2-Myc) that transiently express tHCPro-Myc, HCPro1-Myc, and HCPro2-Myc *in planta*. Briefly, the tHCPro, HCPro1, and HCPro2 coding regions from pF3-tHCPro-P3N were amplified, followed by integration into a binary plant expression vector, pCaMterX (65). Similarly, four additional plasmids, pCaM-N1, pCaM-N2, pCaM-D1, and pCaM-D2, which express the N and D domains of HCPro1 or HCPro2, were constructed.

To determine the repression of the D1 domain on antisilencing activity of HCPro1 N1, the overlapping PCR method was adopted to produce two plasmids, pCaM-N1D2 and pCaM-N2D1, for which the D domains of HCPro1 and HCPro2 were swapped. To investigate whether the detachment of HCPro1 affects antisilencing activity of HCPro2, two derivatives of pCaM-tHCPro-Myc, pCaM-tHCPro(C161A), and pCaM-tHCPro(G273A), for which the *cis*-cleavage of HCPro1 was abolished, were constructed. In brief, two plasmids, pF3-tHCPro-P3N(C161A) and pF3-tHCPro(G273A), were subjected to PCR amplification of tHCPro-P3N(C161A) and tHCPro(G273A), respectively, and the resulting PCR products were cloned into pCaMterX by XhoI/KpnI sites.

For generation of digoxin-labeled *GFP* probe, total RNA was extracted from 16c leaf tissues, followed by RT-PCR amplification of the complete GFP-coding region. The resulting PCR product was ligated into pGEM-T easy vector (Promega) to produce the plasmid pGEM-GFP.

All constructs above were verified by DNA sequencing.

***In vitro* translation.** A WGE-based *in vitro* translation assay was employed to assess the *cis*-cleavage activity of the indicated cysteine proteases or their mutants. For the assay, transcription and translation reactions were coupled using the $T_N T$ SP6 high-yield wheat germ protein expression system and the FluoroTect Green$_{Lys}$ *in vitro* translation labeling system (Promega), essentially following the manufacturer's protocols. Subsequently, an aliquot of 4 μl of translation product for each sample was mixed with 10% SDS protein loading buffer, denatured at 60°C for 10 min, and separated by 12% SDS-polyacrylamide gel electrophoresis (SDS-PAGE). Protein bands were visualized under a fluorescence scanning imager (Typhoon FLA; GE Healthcare).

Sequence analysis. Nucleotide sequence analysis, such as protein sequence deduction, was performed using the Lasergene software package version 7.1. The HCPro sequences (or their truncated versions) of 44 representative species in 10 definitive genera and our recently proposed genus (*Arepavirus*) within the *Potyviridae* family, as previously reported (37, 38), were subjected to pairwise calculation of amino acid sequence identities, multiple alignment, and phylogenetic analysis. The pairwise calculation was carried out via ClustalW2 (https://www.ebi.ac.uk/Tools/msa/clustalw2/). Multiple alignment was performed using ClustalX 1.8.1 (http://www.clustal.org/), followed by the description with the Esprit 3.0 program (http://espript.ibcp.fr/ESPript/ESPript/) (66). A phylogenetic tree was constructed with the maximum-likelihood method using MEGA 7.0.20. The robustness of the inferred evolutionary relationships was assessed by 1,000 bootstrap replicates.

Agroinfiltration assays. Fully expanded leaves from wild-type *N. benthamiana* and 16c line seedlings at the 6- to 8-leaf stage were used for infiltration of *A. tumefaciens* cultures of the strain GV3101 harboring the relevant plasmids by following a previously described protocol (43, 67). For the single-stranded RNA-mediated silencing suppression assay, the classic two-component transient coexpression was performed by agroinfiltration of GFP-expressing construct pCHF3-35S-GFP (35S:GFP) (40) together with any of the tested plasmids. Briefly, two agrobacterial cultures, harboring the 35S:GFP and a candidate protein-expressing construct were adjusted into OD$_{600}$ of 1.0, mixed with equal volume, and coinfiltrated into leaves. GFP fluorescence was monitored with a high-intensity UV lamp (Black-Ray B-100AP, UVP), and the infiltrated leaves were photographed at the indicated dpi. For an infectivity test of ANSSV-derived cDNA clones, agrobacterial culture harboring pSS-I, pSS-I-G, pSS-I-G(Δ1), pSS-I-G(Δ2), pSS-I-G(P1), or pSS-I-G(HCPro) (these constructs are described below) was adjusted to an optical density at 600 nm (OD$_{600}$) of 1.0 and infiltrated into the third newly emerging leaves of *N. benthamiana* seedlings.

Northern blot and siRNA blot analyses. In an RNA silencing suppression assay, Northern blotting was employed to detect the expression of the *GFP* gene. Briefly, total RNA was extracted from fresh leaf tissues using TRIzol (Invitrogen), separated in 1.2% agarose gel containing 2% formaldehyde, and transferred to Hybond-N$^+$ membranes (GE Healthcare) by upward capillary transfer in 20× SSC buffer (1× SSC is 0.15 M NaCl plus 0.015 M sodium citrate). The membranes were hybridized to *GFP*-specific probes labeled with digoxigenin, which was prepared using a DIG Northern starter kit (Roche) with the linearized plasmid pGEM-GFP as the template. The detection of DIG signals was performed using CDP-*star* reagent in the kit. RNA bands were visualized using an ImageQuant LAS 4000 mini biomolecular imager (GE Healthcare) and analyzed with ImageJ software (68) for signal quantification.

The accumulation level of *GFP*-derived siRNAs was detected essentially as previously described (40). In brief, an aliquot of 5 μg of low-molecular-mass RNAs per sample was fractionated on a 15% PAGE containing 7 M urea and transferred to a Hybond-N$^+$ membrane (GE Healthcare) by a semidry transfer instrument (LIUYI). After UV cross-linking and prehybridization, the blots were hybridized with a digoxigenin-labeled *GFP*-specific small RNA probe with an average length of approximately 50 nt, which was prepared by hydrolysis of antisense *GFP* RNA probe with carbonate buffer (23, 69). Detection and imaging of hybridization signals were the same as described above.

Immunoblotting and antibodies. Fresh leaf tissues of *N. benthamiana* were collected at the indicated days and subjected to extraction of total proteins, essentially as described previously (43). Total proteins were separated by 12% SDS-PAGE, electroblotted onto a polyvinylidene difluoride membrane, and detected by immunoblotting using an anti-GFP or anti-Myc polyclonal antibody (Abcam). Goat anti-rabbit immunoglobulin antibody (Abcam) conjugated to horseradish peroxidase was used as the secondary antibody. The blots were treated with enhanced chemiluminescence detection reagents (Thermo Fisher Scientific) and visualized using an ImageQuant LAS 4000 mini biomolecular imager (GE Healthcare).

Construction of ANSSV-derived cDNA clones and infectivity test. Standard DNA manipulation technologies were used to construct a complete cDNA clone of ANSSV-HNBT with a low-copy mini-binary T-DNA vector pCB301 as the backbone (70), essentially as described previously (71). Briefly, a modified pCB301 vector with our desired multiple cloning sites was amplified from pVPH (43). The entire ANSSV genome might be split into four portions (from the 5′ terminus: N1, N2, M, and C) that are delimited with unique MluI, BamHI, and AatII sites (Fig. 9A). Among them, the MluI and AatII sites were artificially created by mutating A (nucleotide position 2566) and T (position 5677) into corresponding G and C during primer synthesis; however, these mutations did not alter the encoded amino acids. The fragments M, C, and N1 were amplified by RT-PCR and integrated, step-by-step, into the modified pCB301 vector with the multiple cloning sites (Fig. 9A) to generate an intermediate vector. To compromise the toxicity of the P3 coding region to *E. coli*, a 220-bp intron 2 of the *NiR* gene of *P. vulgaris* was amplified from pT7-PLDMV-In2 (72) and integrated into the N2 fragment by the overlapping PCR method. The resulting N2 fragment containing the intron was cloned into the above-described intermediate vector by the MluI/BamHI sites. Finally, the entire genomic cDNA of ANSSV-HNBT was placed between the 35S promoter and Nos terminator in the pCB301 backbone to generate the complete cDNA clone of ANSSV (pSS-I) (Fig. 9A and B).

To develop a recombinant infectious ANSSV clone tagged by GFP, a GFP-coding region was inserted into the NIb/CP intercistronic junction. The original cleavage site "ANKEFQ/MD" at the NIb/CP junction, which is proteolytically recognized by NIa-Pro, was engineered into the NIb/GFP and GFP/CP junctions. The complete GFP-coding region was amplified from pVPH-GFP (43), and an overlapping PCR strategy was adopted to construct this clone. Using pSS-I-G as a parental clone, we constructed HCPro1- and HCPro2-deleted ANSSV mutants pSS-I-G(Δ1) and pSS-I-G(Δ2) using the overlapping PCR method. To evaluate whether the HCPro1, HCPro2, and HCPro1-HCPro2 of ANSSV could be replaced by the corresponding counterparts of a heterologous potyvirus and retain viral viability, the P1, HCPro, and P1-HCPro cistrons of TuMV (accession no. EF028235) were amplified from pCBTuMV-GFP/mCherry (73) to create three chimeric ANSSV clones using the overlapping PCR method, pSS-I-G(P1), pSS-I-G(HCPro), and pSS-I-G(P1HCPro), in which HCPro1, HCPro2, and HCPro1-HCPro2 of ANSSV were substituted with the corresponding counterparts P1, HCPro, and P1-HCPro of TuMV, respectively. In addition, we created another chimeric viral clone, pCBTuMV(HCPro1/2), in which the complete P1-HCPro of TuMV was substituted with the HCPro1-HCPro2 of ANSSV. All constructs were confirmed by DNA sequencing.

For plants inoculated with pSS-I or its derivatives, the presence of virus was detected by RT-PCR at the days indicated. Total RNAs were extracted from newly emerging leaves using TRIzol and treated with DNase I. The first-strand cDNAs were generated using the RevertAid First Strand cDNA synthesis kit (Thermo Fisher Scientific) with random hexamer primers, followed by PCR with Phusion high-fidelity DNA polymerase (Thermo Fisher Scientific) to target the ANSSV CP region. To assess whether the intron sequence was spliced in virus progenies of pSS-I, systemic leaves of plants inoculated with pSS-I were subjected to total RNA extraction, followed by RT-PCR detection of the ANSSV P3 region covering the intron sequence. The PCR product was sequenced for confirmation. For plants inoculated with GFP-tagged ANSSV clones, viral infection accompanying the expression of GFP protein was monitored by the UV lamp and Western blot analysis using an anti-GFP polyclonal antibody as described above (Abcam). For plants inoculated with pCBTuMV and pCBTuMV(HCPro1/2), viral infection was detected by RT-PCR to target the TuMV CP region.

H.C., L.Q., W.S., and Z.T. conserved and designed the project. L.Q., W.S., Z.T., and W.H. carried out experiments. H.C. supervised the work. All authors analyzed and discussed the data. H.C., L.Q., W.S., Z.T., A.A.V., and A.W. wrote the manuscript. All the authors reviewed and approved the manuscript. L.Q., W.S., and Z.T. contributed equally to this work.

We declare no conflicts of interest.

REFERENCES

1. Revers F, García JA. 2015. Molecular biology of potyviruses. Adv Virus Res 92:101–199. https://doi.org/10.1016/bs.aivir.2014.11.006.
2. Wylie SJ, Adams M, Chalam C, Kreuze J, López-Moya JJ, Ohshima K, Praveen S, Rabenstein F, Stenger D, Wang A, Zerbini FM, ICTV Report Consortium. 2017. ICTV virus taxonomy profile: *Potyviridae*. J Gen Virol 98:352–354. https://doi.org/10.1099/jgv.0.000740.
3. Valli A, Gallo A, Rodamilans B, López-Moya JJ, García JA. 2018. The HCPro from the *Potyviridae* family: an enviable multitasking helper component that every virus would like to have. Mol Plant Pathol 19:744–763. https://doi.org/10.1111/mpp.12553.
4. Shen W, Shi Y, Dai Z, Wang A. 2020. The RNA-dependent RNA polymerase NIb of potyviruses plays multifunctional, contrasting roles during viral infection. Viruses 12:77. https://doi.org/10.3390/v12010077.
5. Cui H, Wang A. 2019. The biological impact of the hypervariable N-terminal region of potyviral genomes. Annu Rev Virol 6:255–274. https://doi.org/10.1146/annurev-virology-092818-015843.
6. Huth W, Lesemann DE, Paul HL. 1984. Barley yellow mosaic virus: purification, electron microscopy, serology, and other properties of two types of the virus. J Phytopathol 111:37–54. https://doi.org/10.1111/j.1439-0434.1984.tb04240.x.
7. Chung BY, Miller WA, Atkins JF, Firth AE. 2008. An overlapping essential gene in the *Potyviridae*. Proc Natl Acad Sci U S A 105:5897–5902. https://doi.org/10.1073/pnas.0800468105.
8. Olspert A, Chung BY, Atkins JF, Carr JP, Firth AE. 2015. Transcriptional slippage in the positive-sense RNA virus family *Potyviridae*. EMBO Rep 16:995–1004. https://doi.org/10.15252/embr.201540509.
9. Rodamilans B, Valli A, Mingot A, San León D, Baulcombe D, López-Moya JJ, García JA. 2015. RNA polymerase slippage as a mechanism for the production of frameshift gene products in plant viruses of the *Potyviridae* family. J Virol 89:6965–6967. https://doi.org/10.1128/JVI.00337-15.
10. White KA. 2015. The polymerase slips and PIPO exists. EMBO Rep 16:885–886. https://doi.org/10.15252/embr.201540871.
11. Mingot A, Valli A, Rodamilans B, San León D, Baulcombe DC, García JA, López-Moya JJ. 2016. The P1N-PISPO trans-frame gene of sweet potato feathery mottle potyvirus is produced during virus infection and functions as an RNA silencing suppressor. J Virol 90:3543–3557. https://doi.org/10.1128/JVI.02360-15.
12. Untiveros M, Olspert A, Artola K, Firth AE, Kreuze JF, Valkonen JP. 2016. A novel sweet potato potyvirus open reading frame (ORF) is expressed via polymerase slippage and suppresses RNA silencing. Mol Plant Pathol 17:1111–1123. https://doi.org/10.1111/mpp.12366.
13. Valli A, López-Moya JJ, García JA. 2007. Recombination and gene duplication in the evolutionary diversification of P1 proteins in the family *Potyviridae*. J Gen Virol 88:1016–1028. https://doi.org/10.1099/vir.0.82402-0.
14. Susaimuthu J, Tzanetakis IE, Gergerich RC, Martin RR. 2008. A member of a new genus in the *Potyviridae* infects Rubus. Virus Res 131:145–151. https://doi.org/10.1016/j.virusres.2007.09.001.
15. Rohožková J, Navrátil M. 2011. P1 peptidase: a mysterious protein of family *Potyviridae*. J Biosci 36:189–200. https://doi.org/10.1007/s12038-011-9020-6.
16. Rodamilans B, Valli A, García JA. 2013. Mechanistic divergence between P1 proteases of the family *Potyviridae*. J Gen Virol 94:1407–1414. https://doi.org/10.1099/vir.0.050781-0.
17. Liu YP, Peremyslov VV, Medina V, Dolja VV. 2009. Tandem leader proteases of grapevine leafroll-associated virus-2: host-specific functions in the infection cycle. Virology 383:291–299. https://doi.org/10.1016/j.virol.2008.09.035.
18. Csorba T, Kontra L, Burgyan J. 2015. Viral silencing suppressors: tools forged to fine-tune host-pathogen coexistence. Virology 479–480:85–103. https://doi.org/10.1016/j.virol.2015.02.028.
19. Rodamilans B, Shan H, Pasin F, García JA. 2018. Plant viral proteases:

beyond the role of peptide cutters. Front Plant Sci 9:666. https://doi.org/10.3389/fpls.2018.00666.
20. Pasin F, Simón-Mateo C, García JA. 2014. The hypervariable amino-terminus of P1 protease modulates potyviral replication and host defense responses. PLoS Pathog 10:e1003985. https://doi.org/10.1371/journal.ppat.1003985.
21. Shan H, Pasin F, Valli A, Castillo C, Rajulu C, Carbonell A, Simón-Mateo C, García JA, Rodamilans B. 2015. The *Potyviridae* P1a leader protease contributes to host range specificity. Virology 476:264–270. https://doi.org/10.1016/j.virol.2014.12.013.
22. Pasin F, Shan H, García B, Müller M, San León D, Ludman M, Fresno DH, Fátyol K, Munné-Bosch S, Rodrigo G, García JA. 2020. Abscisic acid connects phytohormone signaling with RNA metabolic pathways and promotes an antiviral response that is evaded by a self-controlled RNA virus. Plant Commun 1:100099. https://doi.org/10.1016/j.xplc.2020.100099.
23. Valli A, Martín-Hernández AM, López-Moya JJ, García JA. 2006. RNA silencing suppression by a second copy of the P1 serine protease of cucumber vein yellowing ipomovirus, a member of the family *Potyviridae* that lacks the cysteine protease HCPro. J Virol 80:10055–10063. https://doi.org/10.1128/JVI.00985-06.
24. Giner A, Lakatos L, García-Chapa M, López-Moya JJ, Burgyán J. 2010. Viral protein inhibits RISC activity by argonaute binding through conserved WG/GW motifs. PLoS Pathog 6:e1000996. https://doi.org/10.1371/journal.ppat.1000996.
25. Tatineni S, Qu F, Li R, Morris TJ, French R. 2012. Triticum mosaic poacevirus enlists P1 rather than HC-Pro to suppress RNA silencing-mediated host defense. Virology 433:104–115. https://doi.org/10.1016/j.virol.2012.07.016.
26. Young BA, Stenger DC, Qu F, Morris TJ, Tatineni S, French R. 2012. Tritimovirus P1 functions as a suppressor of RNA silencing and an enhancer of disease symptoms. Virus Res 163:672–677. https://doi.org/10.1016/j.virusres.2011.12.019.
27. Anandalakshmi R, Pruss GJ, Ge X, Marathe R, Mallory AC, Smith TH, Vance VB. 1998. A viral suppressor of gene silencing in plants. Proc Natl Acad Sci U S A 95:13079–13084. https://doi.org/10.1073/pnas.95.22.13079.
28. Kasschau KD, Carrington JC. 1998. A counterdefensive strategy of plant viruses: suppression of posttranscriptional gene silencing. Cell 95:461–470. https://doi.org/10.1016/s0092-8674(00)81614-1.
29. Stenger DC, Hein GL, Gildow FE, Horken KM, French R. 2005. Plant virus HC-Pro is a determinant of *Eriophyid* mite transmission. J Virol 79:9054–9061. https://doi.org/10.1128/JVI.79.14.9054-9061.2005.
30. Valli A, Gallo A, Calvo M, de Jesús Pérez J, García JA. 2014. A novel role of the potyviral helper component proteinase contributes to enhance the yield of viral particles. J Virol 88:9808–9818. https://doi.org/10.1128/JVI.01010-14.
31. García JA, Pallás V. 2015. Viral factors involved in plant pathogenesis. Curr Opin Virol 11:21–30. https://doi.org/10.1016/j.coviro.2015.01.001.
32. Singh K, Wegulo SN, Skoracka A, Kundu JK. 2018. Wheat streak mosaic virus: a century old virus with rising importance worldwide. Mol Plant Pathol 19:2193–2206. https://doi.org/10.1111/mpp.12683.
33. Baulcombe D. 2004. RNA silencing in plants. Nature 431:356–363. https://doi.org/10.1038/nature02874.
34. Li F, Wang A. 2019. RNA-targeted antiviral immunity: more than just RNA silencing. Trends Microbiol 27:792–805. https://doi.org/10.1016/j.tim.2019.05.007.
35. Wu Q, Wang X, Ding SW. 2010. Viral suppressors of RNA-based viral immunity: host targets. Cell Host Microbe 8:12–15. https://doi.org/10.1016/j.chom.2010.06.009.
36. Burgyán J, Havelda Z. 2011. Viral suppressors of RNA silencing. Trends Plant Sci 16:265–272. https://doi.org/10.1016/j.tplants.2011.02.010.
37. Yang K, Ran M, Li Z, Hu M, Zheng L, Liu W, Jin P, Miao W, Zhou P, Shen W, Cui H. 2018. Analysis of the complete genomic sequence of a novel virus, areca palm necrotic spindle-spot virus, reveals the existence of a

new genus in the family *Potyviridae*. Arch Virol 163:3471–3475. https://doi.org/10.1007/s00705-018-3980-x.

38. Yang K, Shen W, Li Y, Li Z, Miao W, Wang A, Cui H. 2019. Areca palm necrotic ringspot virus, classified within a recently proposed genus *Arepavirus* of the family *Potyviridae*, is associated with necrotic ringspot disease in areca palm. Phytopathology 109:887–894. https://doi.org/10.1094/PHYTO-06-18-0200-R.

39. Adams MJ, Antoniw JF, Beaudoin F. 2005. Overview and analysis of the polyprotein cleavage sites in the family *Potyviridae*. Mol Plant Pathol 6:471–487. https://doi.org/10.1111/j.1364-3703.2005.00296.x.

40. Li F, Huang C, Li Z, Zhou X. 2014. Suppression of RNA silencing by a plant DNA virus satellite requires a host calmodulin-like protein to repress RDR6 expression. PLoS Pathog 10:e1003921. https://doi.org/10.1371/journal.ppat.1003921.

41. Li F, Zhao N, Li Z, Xu X, Wang Y, Yang X, Liu SS, Wang A, Zhou X. 2017. A calmodulin-like protein suppresses RNA silencing and promotes geminivirus infection by degrading SGS3 via the autophagy pathway in *Nicotiana benthamiana*. PLoS Pathog 13:e1006213. https://doi.org/10.1371/journal.ppat.1006213.

42. Verchot J, Carrington JC. 1995. Evidence that the potyvirus P1 proteinase functions *in trans* as an accessory factor for genome amplification. J Virol 69:3668–3674. https://doi.org/10.1128/JVI.69.6.3668-3674.1995.

43. Cui H, Wang A. 2016. Plum pox virus 6K1 protein is required for viral replication and targets the viral replication complex at the early stage of infection. J Virol 90:5119–5131. https://doi.org/10.1128/JVI.00024-16.

44. Rajamäki ML, Kelloniemi J, Alminaite A, Kekarainen T, Rabenstein F, Valkonen JP. 2005. A novel insertion site inside the potyvirus P1 cistron allows expression of heterologous proteins and suggests some P1 functions. Virology 342:88–101. https://doi.org/10.1016/j.virol.2005.07.019.

45. Salvador B, Saénz P, Yangüez E, Quiot JB, Quiot L, Delgadillo MO, García JA, Simón-Mateo C. 2008. Host-specific effect of P1 exchange between two potyviruses. Mol Plant Pathol 9:147–155. https://doi.org/10.1111/j.1364-3703.2007.00450.x.

46. Maliogka VI, Salvador B, Carbonell A, Sáenz P, León DS, Oliveros JC, Delgadillo MO, García JA, Simón-Mateo C. 2012. Virus variants with differences in the P1 protein coexist in a Plum pox virus population and display particular host-dependent pathogenicity features. Mol Plant Pathol 13:877–886. https://doi.org/10.1111/j.1364-3703.2012.00796.x.

47. Martínez F, Daròs JA. 2014. Tobacco etch virus protein P1 traffics to the nucleolus and associates with the host 60S ribosomal subunits during infection. J Virol 88:10725–10737. https://doi.org/10.1128/JVI.00928-14.

48. Carbonell A, Dujovny G, García JA, Valli A. 2012. The cucumber vein yellowing virus silencing suppressor P1b can functionally replace HCPro in plum pox virus infection in a host-specific manner. Mol Plant Microbe Interact 25:151–164. https://doi.org/10.1094/MPMI-08-11-0216.

49. Maliogka VI, Calvo M, Carbonell A, García JA, Valli A. 2012. Heterologous RNA-silencing suppressors from both plant- and animal-infecting viruses support plum pox virus infection. J Gen Virol 93:1601–1611. https://doi.org/10.1099/vir.0.042168-0.

50. Ding SW. 2010. RNA-based antiviral immunity. Nat Rev Immunol 10:632–644. https://doi.org/10.1038/nri2824.

51. Pumplin N, Voinnet O. 2013. RNA silencing suppression by plant pathogens: defence, counter-defence and counter-counter-defence. Nat Rev Microbiol 11:745–760. https://doi.org/10.1038/nrmicro3120.

52. Lakatos L, Csorba T, Pantaleo V, Chapman EJ, Carrington JC, Liu YP, Dolja VV, Calvino LF, López-Moya JJ, Burgyan J. 2006. Small RNA binding is a common strategy to suppress RNA silencing by several viral suppressors. EMBO J 25:2768–2780. https://doi.org/10.1038/sj.emboj.7601164.

53. Zhang X, Du P, Lu L, Xiao Q, Wang W, Cao X, Ren B, Wei C, Li Y. 2008. Contrasting effects of HC-Pro and 2b viral suppressors from sugarcane mosaic virus and tomato aspermy cucumovirus on the accumulation of siRNAs. Virology 374:351–360. https://doi.org/10.1016/j.virol.2007.12.045.

54. Várallyay E, Havelda Z. 2013. Unrelated viral suppressors of RNA silencing mediate the control of ARGONAUTE1 level. Mol Plant Pathol 14:567–575. https://doi.org/10.1111/mpp.12029.

55. Ivanov KI, Eskelin K, Bašić M, De S, Lõhmus A, Varjosalo M, Mäkinen K. 2016. Molecular insights into the function of the viral RNA silencing suppressor HCPro. Plant J 85:30–45. https://doi.org/10.1111/tpj.13088.

56. del Toro FJ, Donaire L, Aguilar E, Chung BN, Tenllado F, Canto T. 2017. Potato virus Y HCPro suppression of antiviral silencing in *Nicotiana benthamiana* plants correlates with its ability to bind *in vivo* to 21- and 22-nucleotide small RNAs of viral sequence. J Virol 91:e00367-17. https://doi.org/10.1128/JVI.00367-17.

57. Shan H, Pasin F, Tzanetakis IE, Simón-Mateo C, García JA, Rodamilans B. 2018. Truncation of a P1 leader proteinase facilitates potyvirus replication in a non-permissive host. Mol Plant Pathol 19:1504–1510. https://doi.org/10.1111/mpp.12640.

58. Cheng X, Wang A. 2017. The potyvirus silencing suppressor protein VPg mediates degradation of SGS3 via ubiquitination and autophagy pathways. J Virol 91:e01478-16. https://doi.org/10.1128/JVI.01478-16.

59. Li F, Wang A. 2018. RNA decay is an antiviral defense in plants that is counteracted by viral RNA silencing suppressors. PLoS Pathog 14:e1007228. https://doi.org/10.1371/journal.ppat.1007228.

60. Li F, Zhang C, Li Y, Wu G, Hou X, Zhou X, Wang A. 2018. Beclin1 restricts RNA virus infection in plants through suppression and degradation of the viral polymerase. Nat Commun 9:1268. https://doi.org/10.1038/s41467-018-03658-2.

61. Kasschau KD, Carrington JC. 2001. Long-distance movement and replication maintenance functions correlate with silencing suppression activity of potyviral HC-Pro. Virology 285:71–81. https://doi.org/10.1006/viro.2001.0901.

62. Rodamilans B, Valli A, Mingot A, San León D, López-Moya JJ, García JA. 2018. An atypical RNA silencing suppression strategy provides a snapshot of the evolution of sweet potato-infecting potyviruses. Sci Rep 8:15937. https://doi.org/10.1038/s41598-018-34358-y.

63. Hafrén A, Eskelin K, Mäkinen K. 2013. Ribosomal protein P0 promotes potato virus A infection and functions in viral translation together with VPg and eIF(iso)4E. J Virol 87:4302–4312. https://doi.org/10.1128/JVI.03198-12.

64. Hafrén A, Lõhmus A, Mäkinen K. 2015. Formation of potato virus A-induced RNA granules and viral translation are interrelated processes required for optimal virus accumulation. PLoS Pathog 11:e1005314. https://doi.org/10.1371/journal.ppat.1005314.

65. Wang DJ, Brandsma M, Yin Z, Wang A, Jevnikar AM, Ma S. 2008. A novel platform for biologically active recombinant human interleukin-13 production. Plant Biotechnol J 6:504–515. https://doi.org/10.1111/j.1467-7652.2008.00337.x.

66. Robert X, Gouet P. 2014. Deciphering key features in protein structures with the new ENDscript server. Nucleic Acids Res 42:320–324. https://doi.org/10.1093/nar/gku316.

67. Cui H, Wang A. 2017. An efficient viral vector for functional genomic studies of *Prunus* fruit trees and its induced resistance to plum pox virus via silencing of a host factor gene. Plant Biotechnol J 15:344–356. https://doi.org/10.1111/pbi.12629.

68. Schneider CA, Rasband WS, Eliceiri KW. 2012. NIH Image to ImageJ: 25 years of image analysis. Nat Methods 9:671–675. https://doi.org/10.1038/nmeth.2089.

69. Hamilton AJ, Baulcombe DC. 1999. A species of small antisense RNA in posttranscriptional gene silencing in plants. Science 286:950–952. https://doi.org/10.1126/science.286.5441.950.

70. Xiang C, Han P, Lutziger I, Wang K, Oliver DJ. 1999. A mini binary vector series for plant transformation. Plant Mol Biol 40:711–717. https://doi.org/10.1023/a:1006201910593.

71. Hu W, Qin L, Yan H, Miao W, Cui H, Liu W. 2020. Use of an infectious cDNA clone of pepper veinal mottle virus to confirm the etiology of a disease in *Capsicum chinense*. Phytopathology 110:80–84. https://doi.org/10.1094/PHYTO-08-19-0307-FI.

72. Tuo D, Shen W, Yan P, Li X, Zhou P. 2015. Rapid construction of stable infectious full-length cDNA clone of papaya leaf distortion mosaic virus using in-fusion cloning. Viruses 7:6241–6250. https://doi.org/10.3390/v7122935.

73. Dai Z, He R, Bernards MA, Wang A. 2020. The *cis*-expression of the coat protein of turnip mosaic virus is essential for viral intercellular movement in plants. Mol Plant Pathol 21:1194–1211. https://doi.org/10.1111/mpp.12973.